# Medicinal Chemistry of $\sigma_1$ Receptor Ligands: Pharmacophore Models, Synthesis, Structure Affinity Relationships, and Pharmacological Applications

Frauke Weber and Bernhard Wünsch

## Contents



**Abstract**

In the first part of this chapter, we summarize the various pharmacophore models for $\sigma_1$ receptor ligands. Common to all of them is a basic amine flanked by two hydrophobic regions, representing the pharmacophoric elements. The development of computer-based models like the 3D homology model is described as

F. Weber (✉)
Institute of Pharmaceutical and Medicinal Chemistry, Westfälische Wilhelms-Universität Münster, Corrensstr. 48, Münster 48149, Germany
e-mail: fwebe_01@uni-muenster.de

B. Wünsch
Institute of Pharmaceutical and Medicinal Chemistry, Westfälische Wilhelms-Universität Münster, Corrensstr. 48, Münster 48149, Germany

Cells-in-Motion Cluster of Excellence (EXC 1003 – CIM), University Münster, Münster, Germany


Handbook of Experimental Pharmacology, DOI 10.1007/164_2017_33

well as the first crystal structure of the $\sigma_1$ receptor. The second part focuses on the synthesis and biological properties of different $\sigma_1$ receptor ligands, identified as **1**-**9**. Monocyclic piperazines **1** and bicyclic piperazines **2** and **3** were developed as cytotoxic compounds, thus the $IC_{50}$ values of cell growth and survival inhibition studies are given for all derivatives. The mechanism of cell survival inhibition, induction of time-dependent apoptosis, of compound **ent-2a** is discussed. Experimentally determined $\sigma_1$ affinity shows good correlation with the results from molecular dynamics simulations based on a 3D homology model. Spirocyclic compounds **4** and **5** represent well-established $\sigma_1$ receptor ligands. The homologous fluoroalkyl derivatives **4** have favorable pharmacological properties for use as fluorinated PET tracers. The (S)-configured fluoroethyl substituted compound **(S)-4b** is under investigation as PET tracer for imaging of $\sigma_1$ receptors in the brain of patients affected by major depression. 1,3-Dioxanes **6c** and **6d** display a very potent $\sigma_1$ antagonist profile and the racemic 1,3-dioxane **6c** has high anti-allodynic activity at low doses. The arylpropenylamines **7** are very potent $\sigma_1$ receptor ligands with high $\sigma_1/\sigma_2$ selectivity. The top compound **7g** acts as an agonist as defined by its ability to potentiate neurite outgrowth at low concentrations. Among the morpholinoethoxypyrazoles **8**, **8c** (known as S1RA) reveals the most promising pharmacokinetic and physicochemical properties. Due to its good safety profile, **8c** is currently being investigated in a phase II clinical trial for the treatment of neuropathic pain. The most potent ligand **9e** of 3,4-dihydro-2(1H)-quinolones **9** shows promising anti-nociceptive activity in the formalin test.

**Keywords**

Pharmacological data • Structure ($\sigma_1$) affinity relationships • Synthesis • $\sigma_1$ Receptor ligands • $\sigma_1$ Receptor pharmacophore models

## 1 Introduction

The sigma-1 ($\sigma_1$) receptor is a membrane-bound protein distributed in the central nervous system and in peripheral organs like heart, kidney, and liver (Weissman et al. 1988; Samovilova et al. 1988; Ela et al. 1994). The $\sigma_1$ receptor is mainly localized at the endoplasmic reticulum and the mitochondria-associated membranes. Ruoho et al. have shown that the $\sigma_1$ receptor consists of two transmembrane regions connected by a loop. Both *C*- and *N*-terminus are located extracellularly or in the ER lumen (Chu and Ruoho 2016). Two additional hydrophobic regions of the $\sigma_1$ receptor were identified by Fontanilla et al. named steroid binding domain-like regions (SBDL I and II). With the help of *N*-substituted photoaffinity labels it was shown that the SBDL I overlaps with one of the two transmembrane regions of the $\sigma_1$ receptor forming the ligand-binding domain together with the SBDL II (Ruoho et al. 2012). $\sigma_1$ Receptors were shown to take part in the regulation of ion channels (e.g., $K^+$ and $Ca^{2+}$) and in the modulation of neurotransmitter systems (Lupardus et al. 2000; Hong and Werling 2000; Hayashi

and Su 2007). In the brain, the $\sigma_1$ receptor is particularly well expressed in areas associated with memory and emotion (Mash and Zabetian 1992). Steroids like progesterone (Su et al. 1988; Schwarz et al. 1989) and *N*,*N*-dimethyltryptamine (Fontanilla et al. 2009) were previously discussed to be endogenous ligands but their $\sigma_1$ receptor binding affinities are low compared with those of sphingosines showing high affinity in the low-nanomolar range (Ruoho et al. 2012). Since many centrally active drugs show high $\sigma_1$ affinity, $\sigma_1$ receptors represent promising targets for the research and development of drugs to treat several neurological or neuropsychiatric disorders like depression, psychosis, and cocaine abuse (Hascoet et al. 1995; Matsumoto et al. 2001; Sharkey et al. 1988; Bermack and Debonnel 2001; Ishikawa et al. 2007; Skuza and Rogoz 2006). The fact that many human cancer cell lines show up-regulated levels of $\sigma_1$ receptors brought them into focus for the development of new antitumor drugs and cancer diagnostics (Hashimoto and Ishiwata 2006). Based on various studies, Chen and Pasternak postulated that the $\sigma_1$ receptor functions as an endogenous anti-opioid receptor system (Chien and Pasternak 1993). By investigation of different $\sigma_1$ receptor ligands in animal models it was shown that $\sigma_1$ agonists inhibit morphine-induced analgesia whereas $\sigma_1$ antagonists potentiate opioid induced analgesia (Chien and Pasternak 1994, 1995). The fact that $\sigma_1$ knockout mice show reduced pain response in the formalin test but not hypersensitivity after treatment with capsaicin lead to interest in $\sigma_1$ receptors as a target in the treatment of neuropathic pain (Entrena et al. 2009).

For the development of new potent $\sigma_1$ receptor ligands with high affinity several pharmacophore models have been developed and optimized. Herein the pharmacophore models reported so far are summarized and compared with respect to existing ligands.

## 2 Pharmacophore Models

In 1994, Glennon et al. reported a two-dimensional pharmacophore model based on deconstruction–reconstruction analysis of different flexible $\sigma_1$ receptor ligands. In this model, two hydrophobic regions flanking a basic amine represent the pharmacophoric elements required for high $\sigma_1$ affinity. A distance of 6–10 Å between the amine moiety and the primary hydrophobic region and of 2.5–3.9 Å between the amino group and the secondary hydrophobic region provides optimal binding conditions. The amine could be of primary, secondary, or tertiary nature. In case of a tertiary amine, only small substituents are allowed, whereas the amine could also be part of a ring system (e.g., piperazine ring). The primary hydrophobic region tolerates sterically demanding residues whereas the secondary region favors smaller substituents like a three-carbon chain. As the two hydrophobic binding pockets of the $\sigma_1$ receptor tolerate bulky groups, the size of substituents can vary slightly without decreasing binding affinity (Fig. 1) (Glennon et al. 1994; Glennon 2005).

Laggner et al. presented in 2005 the first computer-aided three-dimensional pharmacophore model (Fig. 2) based on 23 structurally very different $\sigma_1$ ligands.

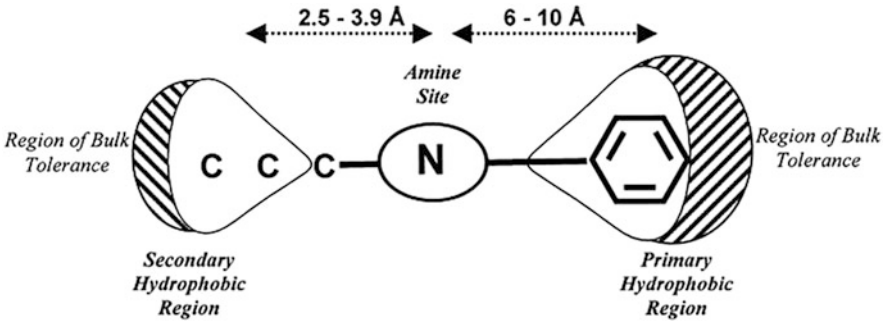


**Fig. 1** Pharmacophore model of Glennon (2005)

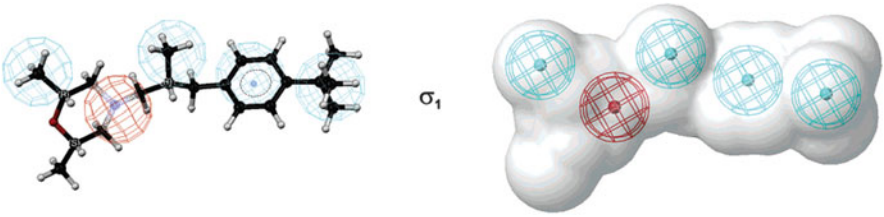


**Fig. 2** 3D-$\sigma_1$-Pharmacophore model of Laggner et al. (2005) *red*: positive ionizable group; *blue*: hydrophobic regions

The pharmacophoric elements consist of a positive ionizable group like an amine and four hydrophobic features. The calculated distances between the pharmacophoric elements are in good agreement with the results obtained by Glennon et al. (1994).

In 2009, Zampieri et al. designed another computer-based model containing five pharmacophoric elements (Fig. 3) (Zampieri et al. 2009). The model included three hydrophobic areas in total (depicted in blue and pink), whereby two of them should have aromatic character (blue). A basic center (red) is located at a distance of 7.01 and 8.50 Å from the aromatic moieties and at a distance of 3.58 Å from the further hydrophobic elements. These distances are comparable to those postulated in the models of Glennon and Laggner. Additionally, the Zampieri model established an H-bond acceptor function, which was already defined in a pharmacophore model by Gilligan et al. This model was published in the early 1990s and did not differentiate between $\sigma_1$ and $\sigma_2$ ligands (Gilligan et al. 1992).

In 2011, Laurini et al. published the first computer-based 3-dimensional (3D) homology model of the $\sigma_1$ receptor. For the identification of a reliable ligand-binding domain, results of docking studies, mutagenesis studies, structure–affinity-relationship studies, and pharmacophore models were combined. The validation of the homology model was implemented by docking studies of well-known $\sigma_1$ ligands at the postulated binding site of the receptor, calculation of free binding

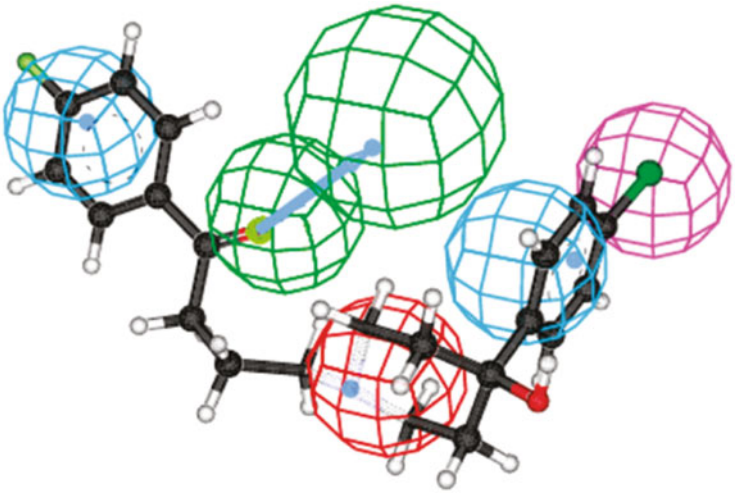

**Fig. 3** Pharmacophore model of Zampieri et al. (2009) *red*: basic center; *green*: H-bond acceptor; *blue*: aromatic hydrophobic area; *pink*: hydrophobic area

energy, and comparison with the experimentally determined $\sigma_1$ affinities of these ligands (Laurini et al. 2011, 2012).

Schmidt et al. have just published a crystal structure of the $\sigma_1$ receptor for the first time (Schmidt et al. 2016). This structure was determined in complex with two different $\sigma_1$ receptor ligands, PD144418 and 4-IBP. Contrary to the early findings of Fontanilla and Ruoho (Ruoho et al. 2012) as well as Aydar et al. only one transmembrane domain of the $\sigma_1$ receptor was found in the crystal structure (Schmidt et al. 2016). This contradicts also the solution nuclear magnetic resonance (NMR) results of Ortega-Roldan et al. (2015) which closely match the findings of the 3D homology model of Laurini et al. (2011).

## 3 Ligands Introduction

In the literature, a great variety of $\sigma_1$ receptor ligand classes are reported. These classes include piperazines **1**, bicyclic compounds of type **2** and **3**, spirocyclic compounds **4** and **5**, 1,3-dioxanes **6**, arylalkenylamines **7**, morpholinoethoxypyrazoles **8**, and 3,4-dihydro-2(1*H*)-quinolones **9** (Fig. 4). The synthesis and the pharmacological properties of these ligands are presented herein.

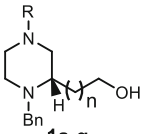

**1a-g**

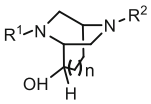

**2a-f**

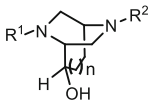

**3a-f**

| | n | R | $K_i(\sigma_1)$ |
|---|---|---|---|
| **1a** | 0 | PMB | 12 nM |
| **1b** | 1 | PMB | 20 nM |
| **1c** | 1 | Me | > 1000 nM |
| **1d** | 1 | $C_6H_{11}CH_2$ | 4.2 nM |
| **1e** | 1 | $C_6H_{11}CH_2$ | 4.7 nM |
| | | Bn = 2-Naph$CH_2$ | |
| **1f** | 2 | $C_6H_{11}CH_2$ | 275 nM |
| **1g** | 3 | $C_6H_{11}CH_2$ | 52 nM |

| | n | $R^1$ | $R^2$ | $K_i(\sigma_1)$ |
|---|---|---|---|---|
| **2a** | 0 | $C_6H_{11}CH_2$ | $PhCH_2$ | 4.8 nM |
| **2b** | 0 | $C_6H_{11}CH_2$ | 1-Naph$CH_2$ | 8.0 nM |
| **2c** | 0 | $C_6H_{11}CH_2$ | 4-Ph-$PhCH_2$ | 9.8 nM |
| **2d** | 1 | $C_6H_{11}CH_2$ | $PhCH_2$ | 6.0 nM |
| **2e** | 1 | PMB | $PhCH_2$ | 125 nM |
| **2f** | 2 | PMB | $PhCH_2$ | 298 nM |

| | n | $R^1$ | $R^2$ | $K_i(\sigma_1)$ |
|---|---|---|---|---|
| **3a** | 0 | $C_6H_{11}CH_2$ | $PhCH_2$ | 6.9 nM |
| **3b** | 0 | $C_6H_{11}CH_2$ | 1-Naph$CH_2$ | 7.1 nM |
| **3c** | 0 | $C_6H_{11}CH_2$ | 4-Ph-$PhCH_2$ | 9.8 nM |
| **3d** | 1 | $C_6H_{11}CH_2$ | $PhCH_2$ | 6.0 nM |
| **3e** | 1 | PMB | $PhCH_2$ | 6.5 nM |
| **3f** | 2 | PMB | $PhCH_2$ | 25 %[a] |

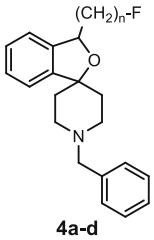

**4a-d**

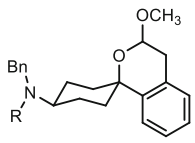

*cis*-**5a-d**

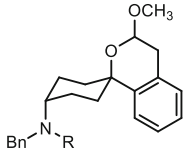

*trans*-**5a**

| | n | $K_i(\sigma_1)$ |
|---|---|---|
| **4a** | 1 | 0.74 nM |
| **4b** | 2 | 0.59 nM |
| **4c** | 3 | 1.4 nM |
| **4d** | 4 | 1.2 nM |

| | R | $K_i(\sigma_1)$ |
|---|---|---|
| *cis*-**5a** | $CH_3$ | 24 nM |
| *cis*-**5b** | $C_2H_5$ | 107 nM |
| *cis*-**5c** | $C_5H_{11}$ | >1000 nM |
| *cis*-**5d** | $PhCH_2$ | >1000 nM |

| | R | $K_i(\sigma_1)$ |
|---|---|---|
| *trans*-**5a** | $CH_3$ | 43 nM |

**6a-d**

| | $R^1$ | $R^2$ | $K_i(\sigma_1)$ |
|---|---|---|---|
| (*S*,*R*)-**6a** | H | H | >10000 |
| (*R*,*R*)-**6b** | $CH_3$ | H | >10000 |
| (*S*,*R*)-**6c** | H | $PhCH_2$ | 6.0 nM |
| (*R*,*R*)-**6d** | $CH_3$ | $PhCH_2$ | 17 nM |

| | $R^1$ | $R^2$ | $K_i(\sigma_1)$ |
|---|---|---|---|
| (*R*,*S*)-**6a** | H | H | >10000 |
| (*S*,*S*)-**6b** | $CH_3$ | H | >10000 |
| (*R*,*S*)-**6c** | H | $PhCH_2$ | 50 nM |
| (*S*,*S*)-**6d** | $CH_3$ | $PhCH_2$ | 11 nM |

**Fig. 4** Representative $\sigma_1$ receptor ligands of different compound classes. Inhibition of $\sigma_1$ receptor radioligand binding at 1 μM concentration of test compound. *PMB* *p*-methoxybenzyl; *Naph* naphthyl

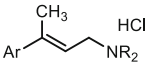

**7a-f·HCl**

| | Ar | $NR_2$ | $K_i(\sigma_1)$ |
|---|---|---|---|
| **7a** | 4-Ph-$PhCH_2$ | piperidine | 0.86 nM |
| **7b** | 2-Naph | piperidine | 0.97 nM |
| **7c** | 4-Ph-$PhCH_2$ | 4-benzylpiperidine | 7.0 nM |
| **7d** | 2-Naph | 4-benzylpiperidine | 23 nM |
| **7e** | 4-Ph-$PhCH_2$ | morpholine | 12 nM |
| **7f** | Ph | morpholine | >1000 nM |

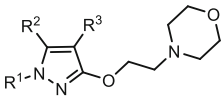

**8a-f**

| | $R^1$ | $R^2$ | $R^3$ | $K_i(\sigma_1)$ |
|---|---|---|---|---|
| **8a** | *tert*-butyl | H | H | >1000 nM |
| **8b** | 4-chlorophenyl | H | H | 18 nM |
| **8c** | 2-Naph | $CH_3$ | H | 17 nM |
| **8d** | 2-Naph | $CH_3$ | $CH_3$ | 139 nM |
| **8e** | 3,4-dichlorophenyl | $CH_3$ | $CH_3$ | 9.4 nM |
| **8f** | 3,4-dichlorophenyl | $CH_3$ | $C(C=O)CH_3$ | 741 nM |

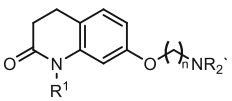

**9a-i**

| | $R^1$ | n | $NR_2$` | $K_i(\sigma_1)$ |
|---|---|---|---|---|
| **9a** | $PhCH_2$ | 2 | morpholine | > 2000 nM |
| **9b** | $PhCH_2$ | 3 | morpholine | 15 nM |
| **9c** | H | 3 | piperidine | 89 nM |
| **9d** | $CH_3$ | 3 | piperidine | 34 nM |
| **9e** | $PhCH_2$ | 3 | piperidine | 1.84 nM |
| **9f** | 4-F-Ph-$CH_2$ | 3 | piperidine | 1.22 nM |
| **9g** | $PhCH_2$ | 4 | morpholine | 60 nM |
| **9h** | $PhCH_2$ | 5 | morpholine | 88 nM |
| **9i** | $PhCH_2$ | 6 | morpholine | 682 nM |

**Fig. 4** (continued)

## 4 Homologous 2-Piperazinealkanols

Piperazines **1** with different hydroxyalkyl side chains represent well-established $\sigma_1$ receptor ligands. A broad structure affinity relationship study was performed based on 2-hydroxyethyl substituted piperazines with high $\sigma_1$ affinity and their larger and smaller homologs bearing hydroxypropyl or hydroxymethyl side chains. The cytotoxic activity against human cancer cell lines was tested by in vitro cell survival assays (Weber et al. 2014; Holl et al. 2012; Bedurftig and Wunsch 2004).

(*S*)-Serine, (*S*)-aspartic acid, and (*S*)-glutamic acid as enantiomerically pure amino acids of nature's chiral pool were used for the synthesis of homologous piperazinealkanols **1a-g**. The first reaction step includes the esterification of the particular amino acid. The dioxopiperazines **11** were prepared from the aminoesters **10**·HCl in a three-step reaction sequence consisting of reductive alkylation, chloroacetylation, and ring closure with different primary amines. Reduction with

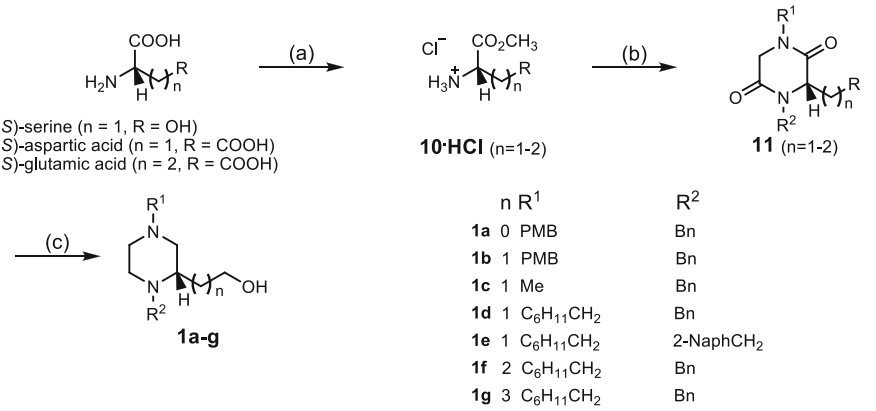


**Scheme 1** Synthesis of homologous 2-piperazinealkanols **1**. Reagents and reaction conditions: (**a**) $(H_3C)_3SiCl$, $CH_3OH$, room temperature (rt), 16 h; (**b**) (1) Ph-CH=O, $NEt_3$, $CH_2Cl_2$, rt, 16 h; (2) $NaBH_4$, $CH_3OH$, 0 °C, 40 min; (3) $ClCH_2COCl$, $NEt_3$, $CH_2Cl_2$, rt, 2.5 h; (4) $R^1$-$NH_2$, $NEt_3$, $CH_3CN$, rt, 16 h–3 d; (**c**) $LiAlH_4$, THF, reflux, 16 h. *PMB* *p*-methoxybenzyl, *2-NaphCH*$_2$ 2-naphthyl (Weber et al. 2014; Holl et al. 2012; Bedurftig and Wunsch 2004)

$LiAlH_4$ led to the piperazinealkanols **1a-g** (Scheme 1). Reduction of the ester moiety of **11d** ($n = 1$, R = $CO_2CH_3$) followed by Wittig reaction of the resulting aldehyde with methyl(triphenylphosphoranylidene)acetate and subsequent reduction of the α,β-unsaturated ester led to the homologous hydroxybutyl piperazine **1g** (Weber 2012).

The $\sigma_1$ and $\sigma_2$ affinity of hydroxyalkyl piperazines **1a-g** was tested with tissue membrane preparations of animal origin (guinea pig brain, rat liver). Selected ligands (**1d-g**) were also assayed with membrane preparations bearing human $\sigma_1$ receptors to evaluate ligand-binding affinity towards $\sigma_1$ receptors from different species (Table 1).

For a high $\sigma_1$ affinity, the length of hydroxyalkyl side chain and the size of the residues at both *N*-atoms are of particular importance. Short side chains like hydroxymethyl and hydroxyethyl are well-tolerated by the $\sigma_1$ receptor leading to $K_i$ values in the range of 4–20 nM. The $\sigma_1$ affinity of the hydroxypropyl piperazines is more than tenfold lower (e.g., **1f**, $K_i = 275$ nM). The extension of the side chain by another methylene moiety in case of hydroxybutyl piperazine **1f** leads to an increased $\sigma_1$ affinity, but the $K_i$ value of 52 nM remained higher than the $K_i$ value measured for hydroxymethyl and hydroxyethyl derivatives. In accordance with the pharmacophore model of Glennon postulating two hydrophobic regions, the *N*-methyl substituted piperazine **1c** does not show high $\sigma_1$ receptor affinity. The affinity increases by the introduction of a larger residue such as cyclohexylmethyl or *p*-methoxybenzyl group.

The hydroxyethyl derivatives show almost the same $\sigma_1$ affinity as the hydroxymethyl derivatives, but show reduced $\sigma_2$ affinity than hydroxyethyl piperazines. Regarding the $\sigma_1/\sigma_2$ selectivity, it becomes clear that the hydroxyethyl

**Table 1** Inhibition of cancer cell growth by piperazinealkanols **1a-g** compared with $\sigma_1$ and $\sigma_2$ binding affinity

| | $\sigma_1$ (gp)[a] $K_i$ [nM] ± SEM | $\sigma_2$ (rat)[b] $K_i$ [nM] ± SEM | $\sigma_1$ (hu)[c] $K_i$ [nM] ± SEM | $\sigma_1$/ $\sigma_2$ selectivity (ratio) | $\sigma_1 K_i$ (calc) [nM] | $IC_{50}$ [μM] RT4[d] | $IC_{50}$ [μM] 5637[e] | $IC_{50}$ [μM] A-427[f] | $IC_{50}$ [μM] LCLC-103H[g] | $IC_{50}$ [μM] DAN-G[h] | $IC_{50}$ [μM] MCF-7[i] | $IC_{50}$ [μM] RPMI 8226[j] |
|---|---|---|---|---|---|---|---|---|---|---|---|---|
| 1a | 12 ± 1.4 | 70 ± 10 | – | 6 | – | – | – | – | – | – | – | – |
| 1b | 20 ± 6.0 | >1,000 | – | 50 | – | – | – | – | – | – | – | – |
| 1c | 28%[k] | 27%[k] | – | – | – | >20 | >20 | >20 | >20 | >20 | >20 | >20 |
| 1d | 4.2 ± 1.1 | 116[l] | 21 ± 4 | 28 | 35 | >20 | >20 | 14 ± 5 | >20 | >20 | 6.8 ± 8.4 | – |
| (*ent*)-1d | 1.9 ± 0.4 | 60 ± 11 | 23 ± 8 | 32 | – | – | >20 | >20 | >20 | >20 | – | >20 |
| 1e | 4.7 ± 1.8 | 69 ± 24 | 6.8 ± 2.3 | 15 | 11 | >20 | 2.1 ± 1.9 | 2.5 ± 2.6 | >20 | >20 | 15 ± 2 | 7.3 ± 3.9 |
| 1f | 275[l] | 690[l] | 71[l] | 3 | – | >20 | 8.0 ± 5.6 | >20 | >20 | >20 | >20 | >20 |
| 1 g | 52[l] | 348[l] | 54 ± 26 | 7 | – | >20 | 6.0 ± 4.0 | 9.6 ± 5.1 | >20 | >20 | >20 | >20 |

[a]Guinea pig brain (gp)
[b]Rat liver (rat)
[c]RPMI 8226 human cancer cell line (hu)
[d]RT4 bladder cancer cell line
[e]Bladder cancer
[f]Small cell lung cancer
[g]Large cell lung cancer
[h]Pancreas cancer
[i]Breast cancer
[j]Multiple myeloma
[k]Inhibition of radioligand binding at 1 μM concentration of test compound (% inhibition)
[l]Result from one measurement. All other results are from three independent experiments

derivatives are more than tenfold selective for the $\sigma_1$ over the $\sigma_2$ receptor. The PMB-substituted compound **1b** provides the best selectivity in this set of compounds with a $\sigma_2$ affinity of >1,000 nM. As a result of further chain extension, the $\sigma_2$ affinity increases leading to decreased selectivity (**1f**, $K_i$ ($\sigma_2$) = 690 nM, **1g**, $K_i$ ($\sigma_2$) = 348 nM).

The $\sigma_1$ affinity of **1d-g** measured with membrane preparations from a human cancer cell line (RPMI 8226) is slightly reduced compared to the affinity measured with the guinea pig brain membrane preparations. Because the same trend was found for the reference compounds haloperidol and (+)-pentazocine it can be assumed that the results of both assays are well comparable.

As the enantiomer of **1d** prepared in the same manner from (*R*)-aspartic acid shows the same $\sigma_1$ affinity, it could be assumed that the stereochemistry has only negligible influence on $\sigma_1$ receptor affinity and selectivity over the $\sigma_2$ subtype ($K_i(\sigma_1)$ = 1.9 nM, $\sigma_1/\sigma_2$ = 32).

The $\sigma_1$ affinity obtained with human receptor preparations was supported by docking of the ligands in the putative binding site of the 3D $\sigma_1$ receptor homology model. The calculated free binding energies are in good accordance with their recorded affinities towards the $\sigma_1$ receptor. For the most potent human $\sigma_1$ receptor ligand **1g** ($K_{i,exp.}$ = 6.8 nM) a $\Delta G_{bind}$ of $-10.85 \pm 0.36$ kcal/mol was calculated which corresponds to an estimated $K_i(\sigma_1)_{calcd}$ value of 11.2 nM, consistent with the experimentally determined $K_i$ values (Weber et al. 2014).

The cell growth inhibition potential of piperazinealkanols **1c-g** was tested in seven human tumor cell lines. The potent $\sigma_1$ receptor ligand **1e** inhibited the growth and survival of the bladder cancer cell line 5637, the small cell lung cancer cell line A427, and the multiple myeloma cell line RPMI 8226 in the low micromolar range. Even at high concentrations (20 μM) of **1e**, a growth inhibition activity could not be found for the bladder cancer cell line RT4, the large cell lung cancer LCLC-103H, and the pancreas cancer cell line DAN-G. Additionally only low activity was found for the breast cancer cell line MCF-7, indicating a selective mechanism of growth and survival inhibition. Further investigation of the mechanism associated with the inhibitory activity of **1e** was performed with RPMI 8226 cells and revealed an increase in the amount of early apoptotic cells after 48 h compared to the untreated control.

## 5 Bicyclic Piperazines

In order to investigate the influence of conformational restriction on $\sigma_1$ receptor affinity bicyclic compounds of type **2** and **3** with diazabicycloalkan scaffold were designed by intramolecular connection of the 2-hydroxyalkyl side chain of piperazines **1** with *C*-5 of the piperazine ring. Propano- and butano-bridged homologs of **2** and **3** with diazabicyclo[3.2.2]nonane and diazabicyclo[4.2.2]decane scaffold were synthesized by an expansion of the ethano-bridge by one or two

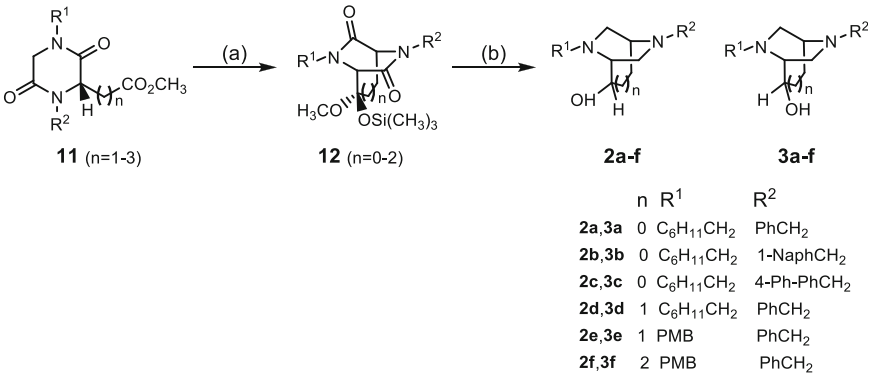


| | n | $R^1$ | $R^2$ |
|---|---|---|---|
| **2a**,**3a** | 0 | $C_6H_{11}CH_2$ | $PhCH_2$ |
| **2b**,**3b** | 0 | $C_6H_{11}CH_2$ | 1-$NaphCH_2$ |
| **2c**,**3c** | 0 | $C_6H_{11}CH_2$ | 4-Ph-$PhCH_2$ |
| **2d**,**3d** | 1 | $C_6H_{11}CH_2$ | $PhCH_2$ |
| **2e**,**3e** | 1 | PMB | $PhCH_2$ |
| **2f**,**3f** | 2 | PMB | $PhCH_2$ |

**Scheme 2** Synthesis of bicyclic diazabicycloalkanols **2** and **3**. Reagents and reaction conditions: (**a**) $n = 1$: NaHMDS, THF, −78 °C, 40 min, then $(H_3C)_3SiCl$, −78 °C, 1 h, then rt, 2 h (Weber et al. 2016); $n = 2$: LiHMDS, THF, −78 °C, 30 min, then $(H_3C)_3SiCl$, −78 °C, 0.5 h, then rt, 3 h (Geiger et al. 2007); $n = 3$: LiHMDS, THF, −78 °C, 30 min, then $(H_3C)_3SiCl$, −78 °C, 2 h, then rt, 0.5 h (Sunnam 2010); (**b**) $n = 0$: 1. 0.5 M HCl, THF, rt, 16 h; 2. $LiAlH_4$, THF, reflux, 16 h (Weber et al. 2016); $n = 1$: 1. *p*-TosOH, THF, $H_2O$, rt, 16 h; 2. $LiBH_4$, THF, −90 °C, 3.5 h; 3. $LiAlH_4$, THF, reflux, **16 h** (Geiger et al. 2007) $n = 2$: 1. *p*-TosOH, THF, $H_2O$, rt, 16 h; 2. $LiBH_4$, THF, −90 °C, 2.5 h; 3. $LiAlH_4$, THF, reflux, 15 h (Sunnam 2010)

methylene moieties to elucidate the effect of bridge size on $\sigma_1$ receptor affinity (Geiger et al. 2007; Weber et al. 2016; Sunnam 2010).

Homologous dioxopiperazines **11** ($n = 1$–3) with different substitution pattern of the *N*-atoms were used as starting material for the synthesis of bicyclic compounds **2** and **3** (Scheme 2). The dioxopiperazine **11** ($n = 3$) was synthesized from racemic-2-aminoadipic acid in the same manner as explained for dioxopiperazines **11** ($n = 1,2$) in Scheme 1. The mixed methyl silyl ketals **12** were obtained by Dieckmann analogous cyclization of **11**. The Dieckmann analogous cyclization gave only low yields for the dioxopiperazines **11** ($n = 1$) with acetate side chain due to the rigidity of the resulting products **12** ($n = 0$). The (*R*)-configuration of the ketalic center of **12** was shown by X-ray crystal structure analysis (Holl et al. 2008). Hydrolysis and reduction of **12** led to the bicyclic alcohols **2** and **3**. The enantiomers *ent*-**2** and *ent*-**3** were obtained starting with (*R*)-configured amino acids.

In piperazinealkanols **1** the hydroxyalkyl side chain can adopt several conformations and, moreover, the piperazine ring can adopt two conformations, leading to an axial or equatorial orientation of the side chain resulting in different distances between the pharmacophoric elements. In the bicyclic alcohols **2** and **3** the additional bridge over the piperazine ring reduces the flexibility of the ring system and its hydroxyalkyl side chain. As a result of conformational restriction, the pharmacophoric elements are fixed in a defined arrangement minimizing the loss of entropy during binding and thus increasing the overall free binding energy.

The $\sigma_1$ and $\sigma_2$ receptor affinity of the bicyclic alcohols **2** and **3** was determined with tissue membrane preparations from guinea pig brain (for $\sigma_1$) and rat liver (for

$\sigma_2$). Compounds **2a-d** and **3a-d** were also tested against human $\sigma_1$ receptors from multiple myeloma RPMI 8226 cell line membrane preparations (Geiger et al. 2007; Weber et al. 2016).

Almost all cyclohexylmethyl substituted compounds **2a-d** and **3a-d** show high $\sigma_1$ receptor affinity with $K_i$ values in the low-nanomolar range. The only exceptions are *ent*-**2a** and **3c**, both with a $K_i$ value of 23 nM. The extension of the ethano-bridge of **2a-c** and **3a-c** by a methylene moiety does not influence $\sigma_1$ receptor affinity since the propane-bridged homologs **2d**,**e** and **3d**,**e** show approximately the same affinity. Only **2e** and *ent*-**2e** show $K_i$ values in the three-digit nanomolar range ($K_i(\sigma_1) = 125$ and 118 nM). However, the introduction of a second methylene moiety leads to a salient decrease in $\sigma_1$ receptor affinity, which implies that butano-bridged diazabicycloalkanols **2f** and **3f** are not tolerated by the $\sigma_1$ receptor.

The stereochemistry has only low impact on $\sigma_1$ receptor affinity since all four stereoisomers **2a,** *ent*-**2a**, **3a,** and *ent*-**3a** show the same $\sigma_1$ receptor affinity. However, in case of PMB-substituted derivatives, **2e** and *ent*-**2e** show lower $\sigma_1$ receptor affinity than **3e** and *ent*-**3e**.

The $\sigma_1$ affinity determined with human $\sigma_1$ receptor material is in good accordance with the $\sigma_1$ affinity obtained with $\sigma_1$ receptors from guinea pig brain.

Compared with the flexible hydroxyethyl piperazines **1b**, **1d,** and **1g**, the corresponding ethano-bridged piperazines **2a-c** and **3a-c** reveal the same $\sigma_1$ receptor affinity. However, the conformational restriction of the hydroxypropyl piperazines **1d** led to increased $\sigma_1$ receptor affinity of **2e** and **3e**. That is due to the higher flexibility of the hydroxypropyl piperazines **1d,e** compared to their shorter hydroxyethyl homologs **1a-d**. This is not valid for the butano-bridged piperazines **2f** and **3f** which display very low $\sigma_1$ affinity, indicating that the bridge size is too bulky for the binding pocket. Obviously the size of the butano-bridge outweighed its positive effect of conformational restriction.

The $\sigma_1/\sigma_2$ selectivity varies from low preference for the $\sigma_1$ receptor (**2c**: $\sigma_1/\sigma_2 = 2$) up to high selectivity for the $\sigma_1$ receptor (**3d**: $\sigma_1/\sigma_2 = 178$). The PMB-substituted derivative *ent*-**3e** ($\sigma_1/\sigma_2 = 227$) showed the highest $\sigma_1/\sigma_2$ selectivity.

The bicyclic compounds **2a-d** and **3a-d** were docked into the binding site of the 3D homology model to determine the free binding energies. Figure 5 illustrates the identified interactions between the high affinity compound *ent*-**3a** ($K_i(\sigma_{1human}) = 1.6$ nM) and the human $\sigma_1$ receptor (Weber et al. 2016).

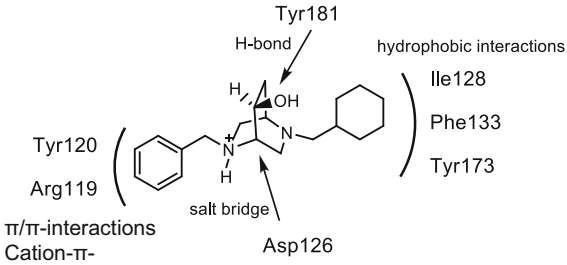


**Fig. 5** Interactions between *ent*-3a and amino acids of the binding site in the 3D homology model of the human $\sigma_1$ receptor

**Table 2** Pharmacological data for diazabicycloalkanols **2** and **3**

| | $\sigma_1$ (gp)[a] $K_i$ [nM] ± SEM | $\sigma_2$ (rat)[b] $K_i$ [nM] ± SEM | $\sigma_1$ (hu)[c] $K_i$ [nM] ± SEM | $\sigma_1$/$\sigma_2$ selectivity | $\sigma_1 K_i$ (calc) [nM] | $IC_{50}$ [μM] RT4[d] | $IC_{50}$ [μM] 5637[e] | $IC_{50}$ [μM] A-427[f] | $IC_{50}$ [μM] LCLC-103H[g] | $IC_{50}$ [μM] MCF-7[h] |
|---|---|---|---|---|---|---|---|---|---|---|
| 2a | 4.8 ± 0.7 | 36 ± 9.0 | 3.2 ± 0.4 | 7 | 19 | >20 | >20 | 16.5 ± 6.2 | >20 | >20 |
| 3a | 6.9 ± 1.6 | 60 ± 26 | 2.4 ± 0.2 | 9 | 22 | >20 | 9.2 ± 6.3 | 9.8 ± 4.3 | >20 | >20 |
| *ent*-2a | 23 ± 13 | 197 ± 18 | 2.8 ± 1.0 | 9 | 12 | >20 | 4.8 ± 3.1 | 2.8 ± 1.7 | >20 | >20 |
| *ent*-3a | 5.7 ± 2.6 | 501 ± 21 | 1.6 ± 0.4 | 88 | 9.7 | >20 | >20 | 11.2 ± 4.8 | >20 | >20 |
| 2b | 8.0 ± 2.0 | 51 ± 16 | 13 ± 5.0 | 6 | 6.3 | 12.9 ± 7.3 | 4.3 ± 1.8 | 2.3 ± 0.9 | 10.4 ± 0.9 | 7.0 ± 4.1 |
| 3b | 7.1 ± 1.8 | 157 ± 21 | 7.2 ± 3.9 | 22 | 8.5 | 11.3 ± 5.9 | 4.9 ± 1.2 | 6.0 ± 3.8 | 8.8 ± 2.0 | 6.8 ± 1.5 |
| 2c | 8.7 ± 1.2 | 20 ± 7.0 | 27 ± 9.0 | 2 | 15 | – | 4.9 ± 4.1 | 1.6 ± 1.2 | 3.2 | – |
| 3c | 23 ± 6.0 | 334 ± 18 | 73 ± 6.0 | 15 | 18 | – | >10 | 4.5 ± 5.7 | >10 | – |
| 2d | 6.0 ± 0.2 | 65 ± 7.0 | 6.4 ± 0.9 | 11 | 20 | >20 | >20 | 7.6 ± 4.7 | >20 | 14 ± 2.8 |
| 3d | 1.6 ± 0.1 | 284 ± 72 | 2.2 ± 1.1 | 178 | 17 | >20 | >20 | 10.3 ± 2.9 | >20 | 16 ± 2.8 |
| 2e | 125 ± 18 | 705[i] | – | 6 | – | 95 ± 14[j] | 103 ± 7.7[j] | 46 ± 11[j] | 96 ± 11[j] | 96 ± 14[j] |
| 3e | 6.5 ± 0.7 | 806[i] | – | 124 | – | 93 ± 10[j] | 88 ± 10[j] | 46 ± 12[j] | 94 ± 6.9[j] | 91 ± 9.4[j] |
| *ent*-2e | 118 ± 5.0 | 441[i] | – | 4 | – | 67 ± 4.2[j] | 88 ± 4.5[j] | 33 ± 7.8[j] | 77 ± 18[j] | 73 ± 9.4[j] |
| *ent*-3e | 7.5 ± 2.1 | 1,700[i] | – | 227 | – | 72 ± 1.2[j] | 72 ± 33[j] | 46 ± 8.6[j] | 80 ± 3.3[j] | 76 ± 1.9[j] |
| 2f | 298 ± 28 | 4,800[i] | – | 162 | – | – | – | – | – | – |
| 3f | 25%[k] | 640[i] | – | – | – | – | – | – | – | – |

[a]Guinea pig brain (gp)
[b]Rat liver (rat)
[c]RPMI 8226 cells (hu)
[d]Bladder cancer
[e]Bladder cancer
[f]Small cell lung cancer
[g]Large cell lung cancer
[h]Breast cancer
[i]Result from one measurement. All other results are from three independent experiments
[j]Relative cell growth (%) in relation to an untreated control
[k]Inhibition of radioligand binding at 1 μM concentration of the test compound

The calculated free binding energies of all docked compounds are in good accordance with the experimentally determined receptor binding data. For *ent*-**3a** the calculated $\Delta G_{bind}$ is $-10.93 \pm 0.34$ kcal/mol corresponding to a calculated $K_i$ value of 9.7 nM. This $K_i$ value is in good agreement with the $K_i$ values recorded with $\sigma_1$ receptors from guinea pig brain ($K_i = 5.7$ nM) and from human RPMI 8226 cell ($K_i = 1.6$ nM) membrane preparations.

The cell growth inhibition potential of compounds **2a-e** and **3a-e** was evaluated in five different cancer cell lines (Table 2). The naphthylmethyl substituted derivatives **2b** and **3b** similarly inhibited the growth and survival of all tested cell lines. The benzyl substituted derivatives **3a** and *ent*-**2a** and the biphenylylmethyl substituted compound **2c** show moderate inhibition of cell growth of the bladder cell line 5637. A clear correlation between $\sigma_1$ receptor affinity and growth and survival inhibition could not be determined, however, we did discern a trend revealing sensitivity of A-427 cell line against all tested bicyclic compounds. With the exception of **2b** and **3b**, growth and survival of the other cell lines were not inhibited at compound concentrations up to 10 or 20 μM.

The bridge size does not show additional influence on $\sigma_1$ receptor affinity. The $K_i$ values of **2d** and **3d** are in the same range as the $K_i$ values of the ethano-bridged compounds **2a-c** and **3a-c**. Although $IC_{50}$ values are not available for compounds **2e** and **3e**, cell growth of only 33–46 % could be detected for the A-427 cell line, whereas the growth of the other cell lines was not inhibited (Geiger et al. 2007).

Further experiments directed to elucidate the mechanism of cell growth inhibition showed that *ent*-**2a** induced apoptosis in A-427 cells in a time-dependent manner (Weber et al. 2016).

## 6 Spirocyclic $\sigma_1$ Receptor Ligands

Spirocyclic compounds **4** represent high affinity $\sigma_1$ receptor ligands with a favorable pharmacological profile for use as fluorinated PET tracers. The homologous fluoroalkyl derivatives **4a-d** bind $\sigma_1$ receptor with $K_i$ values in the low-nanomolar range and show high selectivity over the $\sigma_2$ receptor. The (*S*)-configured fluoroethyl substituted compound (*S*)-**4b** is currently investigated as PET tracer for imaging of $\sigma_1$ receptors in the CNS of patients suffering from major depression (Fischer et al. 2011; Wang et al. 2013; James et al. 2012). The spirocyclic $\sigma_1$ receptor ligands **5** bearing an exocyclic amino moiety allow diverse modifications by the introduction of two *N*-substituents. Furthermore, the existence of cis/trans isomerism increases the diversity of this compound class (Rack et al. 2011).

### 6.1 Homologous Fluoroalkyl Derivatives

The homologous fluoroalkyl derivatives **4a-d** were developed from the 2-benzofuran **15**, a ligand with high $\sigma_1$ receptor affinity ($K_i = 1.1$ nM) and high selectivity over the $\sigma_2$ receptor ($K_i = 1{,}280$ nM) and over 60 other receptors and ion

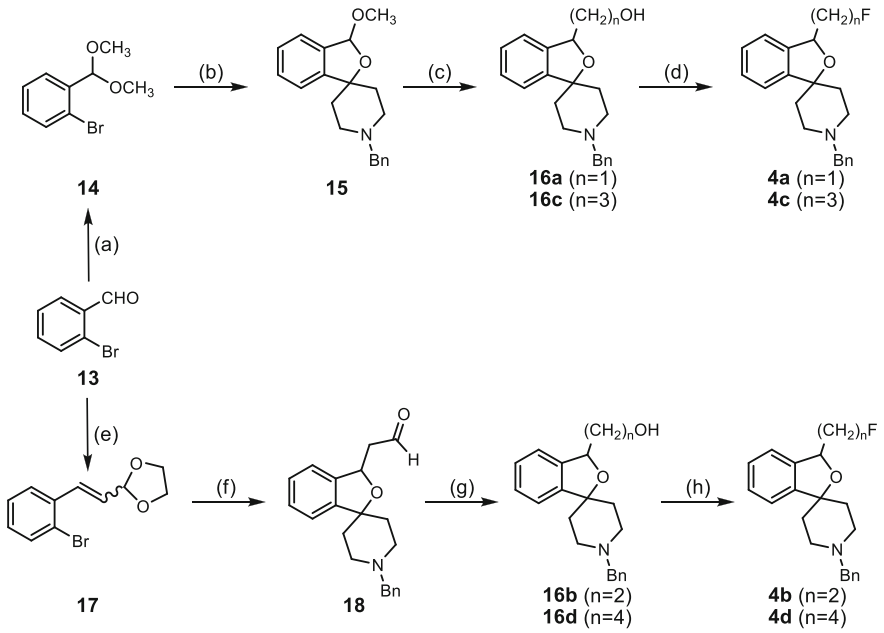


**Scheme 3** Synthesis of homologous fluoroalkyl derivatives **4**. Reagents and reaction conditions (**a**) $HC(OCH_3)_3$, p-TosOH, $CH_3OH$, reflux, 16 h; (**b**) (1) n-BuLi, 1-benzylpiperidin-4-one, THF, −95 °C, 2 h, rt, 4 h; (2) TosOH, $CH_3OH$, rt, 7 d; (Maier and Wunsch 2002a) (**c**) $n = 1$: (1) trimethylsilyl cyanide, tetracyanoethylene, $CH_3CN$, reflux, 4 h; (2) $H_2SO_4$, EtOH, reflux, 7.5 h; (3) $LiAlH_4$, $Et_2O$, −15 °C, 30 min; (Maier and Wunsch 2002a) $n = 3$: (1) allyltrimethylsilane, $BF_3{\cdot}OEt_2$, $CH_2Cl_2$, −25 °C, 20 min, 0 °C, 4 h; (2) 9-BBN, THF, rt, 16 h; (3) $H_2O_2$, NaOH, −25 °C, 45 min, rt 1 h; (Maestrup et al. 2009) (**d**) DAST, $CH_2Cl_2$, −78 °C to rt., 17 h; (Maestrup et al. 2009) (**e**) $[(CH_2O)_2CHCH_2PPh_3Br]$, $K_2CO_3$, TDA-1, $CH_2Cl_2$, reflux, 6 d; (**f**) (1) n-BuLi, THF, 1-benzylpiperidin-4-one, −78 °C, 1 h, rt, 16 h; (2) HCl, THF, rt, 2 h; (**g**) $n = 2$: $NaBH_4$, $CH_3CN$, 0 °C, 15 min, rt, 16 h; (Maestrup et al. 2011) $n = 4$: (1) ethoxycarbonylmethylentriphenylphosphorane, $K_2CO_3$, THF, reflux, 23 h; (2) $H_2$, Pd/C, EtOH, 1 bar, rt, 15 min; (3) $LiAlH_4$, THF, −20 °C, 30 min; (Grosse Maestrup 2010) (h) DAST, $CH_2Cl_2$, −78 °C to rt, 18–21 h (Maestrup et al. 2011)

channels like the hERG $K^+$-channel. To eliminate the metabolically unstable acetalic function and to open up the possibility to introduce a fluorine atom into the molecule, a fluoroalkyl residue was installed instead of the acetalic moiety.

The synthesis of fluoroalkyl derivatives **4a-d** started with the acetalization of 2-bromobenzaldehyde **13** to yield the dimethyl acetal **14** (Scheme 3). Homologation of **13** with a Wittig reagent provided the α,β-unsaturated acetal **17**. Halogen-metal-exchange of the acetals **14** and **17** with *n*-BuLi followed by addition of 1-benzylpiperidin-4-one and subsequent transacetalization afforded the spirocyclic 2-benzofurans **15** and **18**. The 2-benzofuranes **15** and **18** served as key intermediates for the synthesis of alcohols **16**. The alcohols were reacted with diethylaminosulfur trifluoride (DAST) to provide the homologous fluoroalkyl

**Table 3** $\sigma_1$ and $\sigma_2$ binding affinities of homologous fluoroalkyl derivatives **4**

| | *n* | $\sigma_1$ (gp)[a] $K_i$ [nM] ± SEM | $\sigma_2$ (rat)[b] $K_i$ [nM] | $\sigma_1/\sigma_2$ selectivity |
|---|---|---|---|---|
| 4a | 1 | 0.74 ± 0.34 | 550[c] | 743 |
| 4b | 2 | 0.59 ± 0.20 | 785[c] | 1,331 |
| 4c | 3 | 1.4 ± 0.26 | 837[c] | 620 |
| 4d | 4 | 1.2 ± 0.46 | 489[c] | 422 |
| (*S*)-4b | 2 | 2.3 ± 0.2 | 897[c] | 390 |
| (*R*)-4b | 2 | 0.57 ± 0.06 | 1,650[c] | 2,895 |

[a]Guinea pig brain (gp)
[b]Rat liver (rat)
[c]Result from one measurement. All other results are from three independent experiments, and data presented as mean $K_i$ ± SEM (standard error of the mean)

derivatives **4** (Maestrup et al. 2009, 2011; Grosse Maestrup 2010; Maier and Wunsch 2002a, b).

The $\sigma_1$ and $\sigma_2$ receptor affinity of the homologous fluoroalkyl derivatives **4** was determined with receptor material from guinea pig brain ($\sigma_1$) and rat liver ($\sigma_2$).

All four fluoroalkyl homologs **4a-d** bind with very high affinity to the $\sigma_1$ receptor ($K_i(\sigma_1) = 0.59–1.4$ nM) with high selectivity over the $\sigma_2$ subtype (Table 3). The fluoroethyl derivative **4b**, termed fluspidine, shows the most promising ligand-binding profile [$K_i$ ($\sigma_1$) = 0.59 nM, $K_i$ ($\sigma_2$) = 785 nM)].

All four compounds **4a-d** were also synthesized in their [$^{18}$F]-labeled form for the use as PET tracers. For radiosynthesis, the alcohols **14** were transformed into the corresponding tosylates. Nucleophilic substitution of the tosylates with K[$^{18}$F]F complexed with the cryptand Kryptofix 2.2.2 led to the [$^{18}$F] labeled spirocyclic $\sigma_1$ receptor ligands [$^{18}$F]**4a-d** with high radiochemical purity (>98%) and radiochemical yield (40–50%) with reaction times <30 min (Fischer et al. 2011; Maestrup et al. 2009; Maisonial et al. 2011, 2012). Because of the high target affinity and selectivity, [$^{18}$F]**4b** was further evaluated in animal studies with female CD-1 mice. [$^{18}$F]**4b** showed fast and sufficient brain uptake (3.9 and 4.7%ID/g) and high metabolic stability in vivo (>94% parent compound in plasma samples after 30 min, only one metabolite was found). Good concordance between expression of $\sigma_1$ receptors and binding site occupancy with [$^{18}$F]**4b** was found by ex vivo brain section imaging (Fischer et al. 2011). Due to the promising properties of the racemic compound [$^{18}$F]**4b**, the enantiomers (*R*)- and (*S*)-[$^{18}$F]**4b** were separated by chiral HPLC of the tosylate **13b** (Holl et al. 2013). The $\sigma_1$ receptor affinity was 0.57 nM for (*R*)-[$^{18}$F]**4b** and 2.3 nM for (*S*)-[$^{18}$F]**4b**. Thus, the (*R*)-enantiomer is the eutomer.

## 6.2 Spirocyclic Ligands with Exocyclic Amino Moiety

For the synthesis of spirocyclic ligands with exocyclic amino moiety, the dimethyl acetal **19** was reacted in a bromine lithium exchange to give an aryllithium

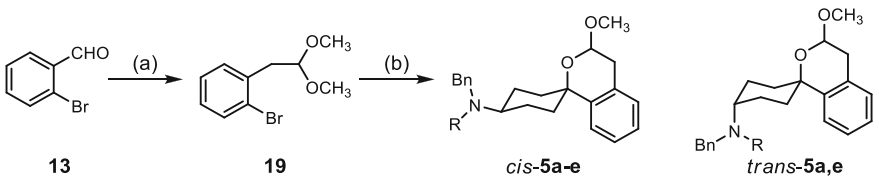


**Scheme 4** Synthesis of spirocyclic ligands **5** with exocyclic amino moiety. Reagents and reaction conditions (**a**) (1) (methoxymethyl)triphenylphosphonium chloride, KO$^t$Bu, THF, −10 °C, then rt, 16 h; (2) *p*TosOH·$H_2O$, MeOH, reflux, 72 h; (**b**) (1) *n*-BuLi, THF, −78 °C, 20 min; (2) cyclohexane-1,4-dione, −78 °C, 2 h, rt, 1 h; (3) $CHCl_3$, HCl, rt, 1.5 h; (4) benzylamine, THF, HOAc, $NaBH(OAc)_3$, rt, 2 h; (5) R-CHO, $NaBH(OAc)_3$, $CH_2Cl_2$, rt, 23 h (Rack et al. 2011)

**Table 4** $\sigma_1$ and $\sigma_2$ binding affinity of spirocyclic ligands **5** with exocyclic amino moiety

| | R | $\sigma_1$ (gp)[a] $K_i$ [nM] ± SEM | $\sigma_2$ (rat)[b] $K_i$ [nM] ± SEM | $\sigma_1/\sigma_2$ selectivity |
|---|---|---|---|---|
| *cis*-5a | $CH_3$ | 24 ± 4.7 | 329[c] | 14 |
| *trans*-5a | $CH_3$ | 43 ± 18 | >1,000 | 23 |
| *cis*-5b | $C_2H_5$ | 107 ± 25 | 666 ± 106 | 6 |
| *cis*-5c | $C_5H_{11}$ | >1,000 | 719[c] | – |
| *cis*-5d | $PhCH_2$ | >1,000 | >1,000 | – |

[a]Guinea pig brain (gp)
[b]Rat liver (rat)
[c]Result from one measurement. All other results are from three independent experiments, and data presented as mean $K_i$ ± SEM (standard error of the mean)

intermediate. After addition to cyclohexane-1,4-dione followed by transacetalization under acidic conditions, reductive amination with benzylamine and $NaBH(OAc)_3$ led to the diastereomeric benzylamines *cis*-**5e** and *trans*-**5e** (R = H, Scheme 4). In order to investigate the influence of the second *N*-substituent, the benzylamines **5e** were transformed into different tertiary amines. Each isomer can adopt different conformations with axially or equatorially oriented amino substituents.

The $\sigma_1$ and $\sigma_2$ receptor affinity of spirocyclic ligands with exocyclic amino moiety **5** was determined with membrane preparations obtained from guinea pig brain (for $\sigma_1$) and rat liver (for $\sigma_2$) (Table 4).

The shift of the basic amino group to a position outside of the spirocyclic ring was envisaged to come closer to the required distances between the pharmacophoric elements (benzene ring and amino moiety) according to the models of Glennon and Laggner. The benzylpiperidin **15** (Fig. 6) shows high $\sigma_1$ receptor affinity and high selectivity over the $\sigma_2$ subtype and over other receptors and ion channels. It was found that small residues at the *N*-atom resulted in low $\sigma_1$ affinity whereas a benzyl group turned out to be optimal. The important role of the *N*-benzyl moiety can be explained by the pharmacophore model of Glennon et al. The benzene ring of the annulated pyrane ring interacts with the primary

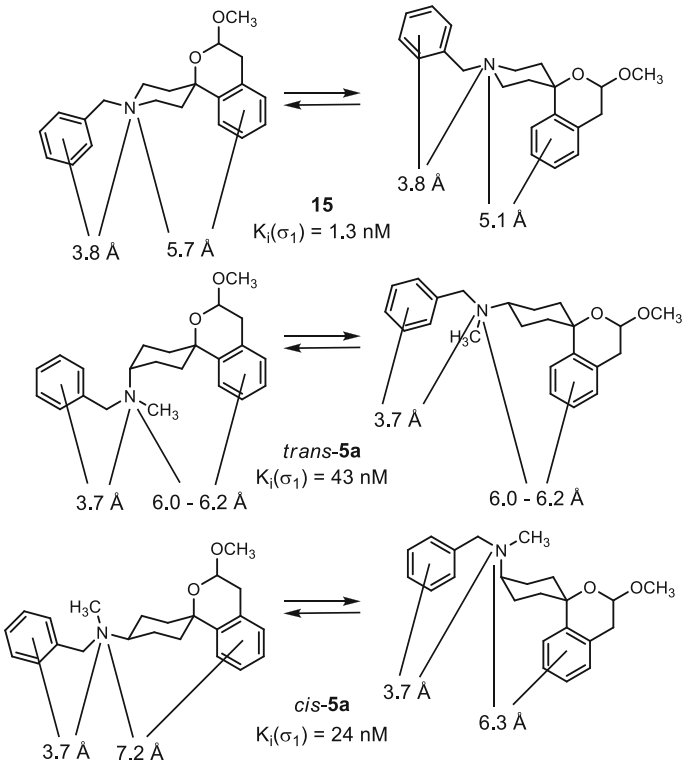


**Fig. 6** Distance calculation of spirocyclic $\sigma_1$ receptor ligands with endocyclic *N* (**15**) and exocyclic amino moiety (*trans*-**5a** and *cis*-**5a**)

hydrophobic region and the benzyl moiety of the *N*-atom interacts with the secondary hydrophobic region. However, the distance between the *N*-atom and the primary hydrophobic region was too small for both conformers with axially and equatorially oriented phenyl ring. Ideally, the distance should be 6–10 Å due to the pharmacophore model of Glennon et al. In case of **15** the distance was found to be 5.7 and 5.1 Å for the equatorial and axial conformer, respectively (Fig. 6). Therefore it was decided to extend the distance between the *N*-atom and the *O*-heterocycle-annulated benzene ring by exclusion of the *N*-atom from the piperidine ring, resulting in spirocyclic compounds **5** with exocyclic amino group. Another advantage of an exocyclic amino moiety is the possibility to install and to modify two different residues at the *N*-atom.

As a result of the shift of the basic group, the distances between the *N*-atom and the *O*-heterocycle-annulated benzene ring of *cis*-**5a** and *trans*-**5a** are in good concordance with the distances postulated by Glennon et al. However, the decrease in $\sigma_1$ affinity ($K_i(\sigma_1) = 24$ and 43 nM) (Rack et al. 2011) provides an example of how receptor binding affinity does not strictly correspond with pharmacophore

models. Other considerations like entropic factors should be noted. The introduction of the benzylamino moiety leads to an increased flexibility of the *N*-substituent.

The $\sigma_1$ receptor affinity of **5** also depends on the second *N*-substituent. Only small groups are tolerated. For small methyl and ethyl groups, the $K_i$ values are 24 and 107 nM, respectively. Bulky residues like pentyl- or benzyl substituents lead to a salient decrease in $\sigma_1$ binding affinity ($K_i(\sigma_1) > 1{,}000$ nM). Generally, *cis*-configured diastereomers show higher $\sigma_1$ binding affinity than their *trans*-configured diastereomers.

## 7 1,3-Dioxanes

Racemic 1,3-dioxane **6c** represents a very potent $\sigma_1$ receptor antagonist (Utech et al. 2011). With these compounds $\sigma_1$ binding affinity depends on the relative configuration of the substituents at the 2- and 4-position, size of the oxygen containing heterocycle, and length of the aminoalkyl side chain. Since the racemic compound **6c**, consisting of a six-membered *O*-heterocycle combined with an aminoethyl side chain, was found to be a promising candidate as $\sigma_1$ receptor ligand, the enantiomers were synthesized and their pharmacology evaluated.

For the synthesis of enantiomerically pure 1,3-dioxanes **6**, the enantiomeric azidodiols (*S*)-**22** and (*R*)-**22** were prepared from diester **20** in high enantiomeric excess (Scheme 5). After silylation of **20** and subsequent reduction, the resulting diol **21** was converted into the azidodiols (*S*)-**22** and (*R*)-**22** following two different pathways using lipases as chiral catalysts. Stereoselective acetalization of (*S*)-**22** and (*R*)-**22** with benzaldehyde or acetophenone led to enantiomerically pure azido-

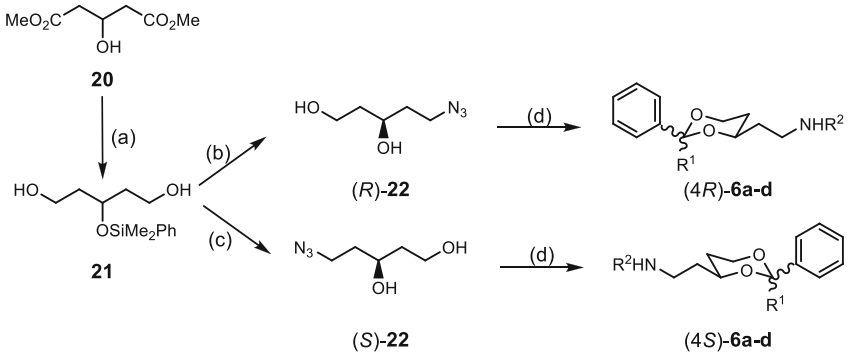


**Scheme 5** Synthesis of enantiomerically pure 1,3-dioxanes **6**. Reagents and reaction conditions. (**a**) (1) $Me_2PhSiCl$, imidazole, $CH_2Cl_2$; (2) $LiBH_4$, $Et_2O$; (**b**) (1) IPA, lipase *Candida Antarctica* B, MTBE; (2) lipase *Burkholderia cepacia*, $NaHCO_3$; (3) $Zn(N_3)_2{\cdot}(pyridine)_2$, DIAD, $PPh_3$, toluene; (4) $K_2CO_3$, $CH_3OH$; (5) HCl; (**c**) (1) IPA, lipase *Burkholderia cepacia*, MTBE; (2) $Zn(N_3)_2{\cdot}(pyridine)_2$, DIAD, $PPh_3$, toluene; (3) $K_2CO_3$, $CH_3OH$; (4) HCl; (Kohler and Wunsch 2006, 2012) (**d**) (1) Ph-C(=O)$R^1$, pTosOH, toluene, Dean Stark apparatus, 4 h; (2) $H_2$, Pd/C, rt, 5 h; $R^2 = PhCH_2$: (3) benzaldehyde, $NaBH(OAc)_3$, $CH_2Cl_2$, rt, 16 h (Kohler et al. 2012). *IPA* isopropenyl acetate, *MTBE* methyl *tert*-butyl ether, *DIAD* diisopropyl azodicarboxylate

**Table 5** $\sigma_1$ and NMDA receptor binding affinities of 1,3-dioxanes **6a-d**

| | $R^1$ | $R^2$ | $\sigma_1$ (gp)[a] $K_i$ [nM] ± SEM | NMDA (p)[b] $K_i$ [nM] ± SEM |
|---|---|---|---|---|
| (*S*,*R*)-6a | H | H | >10,000 | >10,000 |
| (*R*,*S*)-6a | H | H | >10,000 | >10,000 |
| (*R*,*R*)-6b | $CH_3$ | H | >10,000 | 46 ± 17 |
| (*S*,*S*)-6b | $CH_3$ | H | >10,000 | 6,120 ± 630 |
| (*S*,*R*)-6c | H | $PhCH_2$ | 6.0 ± 1.0 | >10,000 |
| (*R*,*S*)-6c | H | $PhCH_2$ | 50 ± 19 | >10,000 |
| (*R*,*R*)-6d | $CH_3$ | $PhCH_2$ | 17 ± 2 | >10,000 |
| (*S*,*S*)-6d | $CH_3$ | $PhCH_2$ | 11 ± 3 | >10,000 |

[a]Guinea pig brain (gp)
[b]Pig brain cortex (p)

1,3-dioxanes, which were subsequently reduced with $H_2$ and Pd/C to obtain the primary amines **6a** and **6b**. Further functionalization of the amino moiety was performed by reductive monobenzylation with benzaldehyde and $NaB(OAc)_3$ to yield the benzylamines **6c** and **6d**.

The $\sigma_1$ and $\sigma_2$ receptor affinity of 1,3-dioxanes **6** was determined with tissue membrane preparations from guinea pig brain (for $\sigma_1$) and rat liver (for $\sigma_2$). The 1,3-dioxanes **6** were also tested against the PCP binding site of the NMDA receptor using pig brain cortex membrane preparations (Table 5).

We found that both enantiomers of the primary amines **6a** and **6b** do not bind $\sigma_1$ ($K_i(\sigma_1) > 10{,}000$ nM) in this assay. According to the pharmacophore model of Glennon et al. (Glennon 2005; Glennon et al. 1994) affinity for $\sigma_1$ should increase by introducing an *N*-benzyl group as a second hydrophobic residue flanking the basic amino moiety as it is shown for the secondary amines **6c** and **6d**. In the case of benzylamines the orientation of the phenyl ring at the 1,3-dioxane ring has minimal influence on $\sigma_1$ affinity as **6a** and **6b** show comparable $K_i$ values of 6.0 and 17 nM for the (4*R*)-configured enantiomers and 50 and 11 nM for the (4*S*)-configured enantiomers. Compound (*S*,*R*)-**6c** with equatorially oriented 2-phenyl moiety shows high $\sigma_1$ affinity ($K_i(\sigma_1) = 6.0$ nM).

Regarding $\sigma_1/\sigma_2$ selectivity, we found that primary amines **6a** and **6b** do not bind $\sigma_1$ and the benzyl amines **6c** and **6d** bind $\sigma_2$ with low affinity ($K_i(\sigma_2) > 200$ nM).

Depending on the absolute configuration the primary amines **6b** with axially oriented phenyl moiety reveal high affinity to the PCP binding site of the NMDA receptor with $K_i$ values of 46 nM ((*R*,*R*)-**6b**) but only 6,120 nM for (*S*,*S*)-**6b**, respectively. The equatorial orientation of the phenyl ring (**6a**) as well as the introduction of a benzyl group at the amino moiety (**6c** and **6d**) led to complete loss of NMDA affinity ($K_i$(NMDA) > 10,000 nM).

The benzyl substituted 1,3-dioxane (*S*,*R*)-**6c** represents the most potent candidate among the secondary amines with high $\sigma_1$ affinity ($K_i(\sigma_1) = 6.0$ nM) and high selectivity over the $\sigma_2$ subtype and the NMDA receptor.

In further studies performed with racemic **6c** ($K_i(\sigma_1) = 19$ nM), promising results were obtained in a capsaicin-induced pain assay with mice. In these studies,

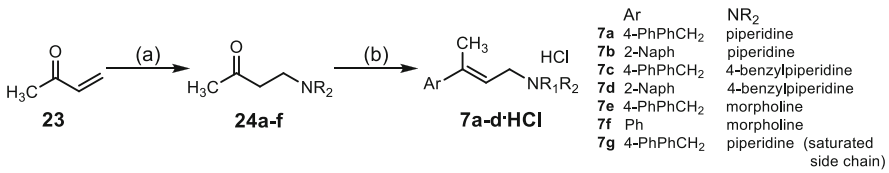


**Scheme 6** Synthesis of arylalkenylamines **7a-f**. Reagents and reaction conditions (**a**) $HNR_2$, PEG 400, rt; (**b**) (1) Ar-Br, t-BuLi, $Et_2O$, −78 °C to rt; (2) 37% HCl, rt; (3) 1 M NaOH; (4) 37% HCl, rt; (5) crystallization from acetone (Rossi et al. 2011). *Naph* naphthyl

**Table 6** $\sigma_1$ and $\sigma_2$ affinity of arylalkenylamines **7a-g**

| | $\sigma_1$ (gp)[a] $K_i$ [nM] ± SEM | $\sigma_2$ (rat)[b] $K_i$ [nM] ± SEM | $\sigma_1$/ $\sigma_2$ selectivity | clog*P* | clogD | MW |
|---|---|---|---|---|---|---|
| 7a | 0.86 ± 0.4 | 111 ± 21 | 129 | 5.32 | 3.82 | 291.43 |
| 7b | 0.97 ± 0.3 | 35 ± 9 | 36 | 4.66 | 3.07 | 265.39 |
| 7c | 7.0 ± 0.9 | 18 ± 1.7 | 3 | 7.19 | 5.60 | 381.55 |
| 7d | 23 ± 2.6 | 16 ± 1.1 | 1 | 6.53 | 4.86 | 355.52 |
| 7e | 12 ± 2.0 | 386 ± 27 | 33 | 4.25 | 4.17 | 293.40 |
| 7f | >1,000 | >1,000 | – | 2.61 | 2.51 | 217.31 |
| 7 g | 0.70 ± 0.3 | 103 ± 10 | 147 | 5.43 | 3.00 | 293.45 |

[a]Guinea pig brain
[b]Rat liver

even a very low dose of 0.25 mg/kg, *rac*-**6c** has high anti-allodynic activity (Utech et al. 2011).

## 8 Arylalkenylamines

Arylpropenylamines of type **7** show high $\sigma_1$ binding affinity and high $\sigma_1/\sigma_2$ selectivity. The influence of the novel $\sigma_1$ ligands on nerve growth factor (NGF)-induced neurite outgrowth was evaluated in the in vitro PC12 cell neurite sprouting assay.

Michael addition of cylic amines to unsaturated ketone **23** led to the β-aminoketones **24**. Subsequent nucleophilic aryllithium addition followed by dehydration with HCl provided the arylalkenylamines **7**, which were crystallized as HCl salts (*E*)-**7a-f** (Scheme 6). The racemic arylalkylamine **7g** was obtained by catalytic hydrogenation of **7a**.

The $\sigma_1$ and $\sigma_2$ receptor binding affinity of compounds **7a-g**·HCl was tested using guinea pig brain (for $\sigma_1$) and rat liver (for $\sigma_2$) membrane preparations. Additionally, the selectivity towards the PCP binding site of the NMDA receptor and against μ- and κ-opioid receptors was determined (Table 6).

Piperidinyl substituted compounds **7a** and **7b** reveal high $\sigma_1$ receptor affinity independent of the aromatic residue ($K_i(\sigma_1)$ = 0.86 and 0.97 nM). Interestingly, naphthalen-2-yl- or biphenyl-4-yl residues appear to be important for high $\sigma_1$

binding affinity of morpholinyl substituted compounds since only low $\sigma_1$ affinity is found when a phenyl substituent is present as aromatic moiety (**7f**, $K_i(\sigma_1)$ >1,000 nM). The tested compounds show high selectivity over the $\sigma_2$ receptor subtype, opioid receptors, and NMDA receptors (the PCP binding site). High $\sigma_2$ binding affinity was found only for 4-benzylpiperidinyl substituted derivatives **7c** and **7d,** with $K_i$ values of 18 and 16 nM, respectively. **7a** represents the most potent and selective $\sigma_1$ receptor ligand of this set of compounds ($K_i(\sigma_1) = 0.86$ nM, $\sigma_1/\sigma_2 = 129$). Therefore the corresponding arylalkylamine **7g** was included in this study. Receptor binding studies revealed similar $\sigma_1$ binding affinity ($K_i(\sigma_1) = 0.70$ nM) and selectivity ($\sigma_1/\sigma_2 = 147$) (Rossi et al. 2011).

clog*P* and clog*D* values were calculated for **7a-g.** Their drug-like properties were confirmed according to Lipinski's "rule of five." With the exception of **7c** (log*D* > 5) all compounds fulfill the "rule of five," i.e., clogD <5, molecular weight < 500, H-bond acceptors <10, and H-bond donors <5.

In order to determine whether the top compounds **7a** and **7g** function as agonists or antagonists their influence on nerve growth factor (NGF)-induced neurite outgrowth in PC12 cells was evaluated. **7g** potentiated the neurite outgrowth at lower concentrations, consistent with agonist activity. This effect was blocked by co-treatment with the $\sigma_1$ receptor antagonist BD-1063, demonstrating the participation of $\sigma_1$ receptors. In contrast, (*E*)-**7a** did not significantly increase neurite sprouting (Rossi et al. 2011).

## 9 Morpholinoethoxypyrazoles

Substituted 1-arylpyrazoles with a basic amino function represent a promising class of $\sigma_1$ receptor antagonists. For high $\sigma_1$ binding affinity, the distance between the basic amino moiety and the pyrazole ring is of major importance. In previous studies an ethylenoxy spacer and a morpholino residue as the *N*-component resulted in high $\sigma_1$ affinity and excellent selectivity over the $\sigma_2$ subtype.

For the synthesis of morpholinoethoxypyrazoles **8a-f**, the 3-hydroxypyrazole **28** was prepared in a two-step reaction sequence starting from arylhydrazines **25**. At first the terminal amino group of hydrazines **25** was protected by acetylation (Scheme 7). Reaction of **26** with β-ketoesters **27** led to the 3-hydroxypyrazoles **28** with high regioselectivity. Subsequent reaction with 4-(2-chloroethyl)morpholine provided the morpholinoethoxypyrazoles **8a-f** (Diaz et al. 2012).

The $\sigma_1$ and $\sigma_2$ binding affinity of morpholinoethoxypyrazoles **8a-f** was determined with human $\sigma_1$ receptors (from transfected HEK-293 cell membrane preparations) and membrane preparations from guinea pig brain (for $\sigma_2$).

Generally, the morpholinoethoxypyrazoles **8a-f** show only very low affinity for the $\sigma_2$ receptor. Affinity for $\sigma_1$ depends on the substitution pattern of the pyrazole ring. Substitution at position 1 with aromatic residues (**8b-f**) produces high $\sigma_1$ binding affinity. Non-aromatic residues (*tert*-butyl, **8a**) produce a salient decrease in $\sigma_1$ binding affinity (Table 7). Only small residues (e.g., $CH_3$, H) are tolerated at 4- and 5-position of the pyrazole ring. In the naphthyl series even a methyl group in

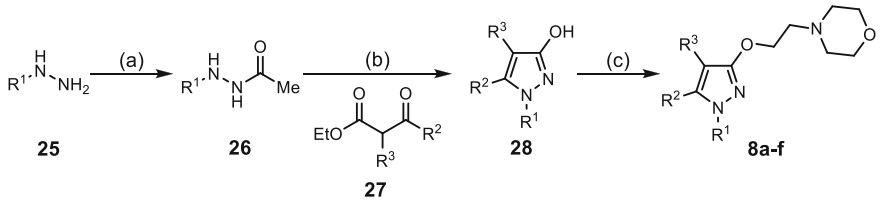


**Scheme 7** Synthesis of morpholinoethoxypyrazoles **8a-f**. Reagents and reaction conditions (**a**) $Ac_2O$, toluene, rt; (**b**) $PCl_3$, 50 °C, 2 h; NaH, DMF, 60 °C, 4 h; (**c**) 4-(2-chloroethyl)morpholine, $K_2CO_3$, NaI, DMF, 95 °C, 18 h (Diaz et al. 2012)

**Table 7** $\sigma_1$ and $\sigma_2$ binding affinity of morpholinoethoxypyrazoles **8a-f**

| | $R^1$ | $R^2$ | $R^3$ | $\sigma_1$ (h)[a] $K_i$ [nM] ± SEM | $\sigma_2$ (gp)[b] $K_i$ [nM] ± SEM | $\sigma_1$/ $\sigma_2$ selectivity |
|---|---|---|---|---|---|---|
| 8a | *tert*-butyl | H | H | >1,000 | >1,000 | – |
| 8b | 4-Chlorophenyl | H | H | 18 ± 1.5 | 357 ± 357 | 20 |
| 8c | 2-Naph | $CH_3$ | H | 17 ± 7.0 | >1,000 | – |
| 8d | 2-Naph | $CH_3$ | $CH_3$ | 139 ± 9 | >1,000 | – |
| 8e | 3,4-Dichlorophenyl | $CH_3$ | $CH_3$ | 9.4 ± 1.8 | 351 ± 400 | 37 |
| 8f | 3,4-Dichlorophenyl | $CH_3$ | C(=O) $CH_3$ | 741 ± 134 | >1,000 | – |

[a]Human $\sigma_1$ receptor from transfected HEK-293 cell membrane preparations (h)
[b]Guinea pig brain membrane preparations (gp)

position 4 seems to be detrimental for high $\sigma_1$ affinity (**8d**, $K_i(\sigma_1) = 139$ nM). The introduction of larger moieties in position 4 (e.g., **8f**, C(=O)Me) produces a salient decrease in $\sigma_1$ binding affinity ($K_i(\sigma_1) = 741$ nM). The 5-alkoxy regioisomer of the most promising ligand **8c** ($K_i(\sigma_1) = 17$ nM) shows a complete loss of $\sigma_1$ affinity ($K_i > 1{,}000$ nM) (Diaz et al. 2012).

The high $\sigma_1$ binding affinity of naphthylpyrazole **8c** (also known as S1RA and E-52862) cannot be explained completely by the common pharmacophore models. The 2-[1-(2-naphthyl)pyrazol-3-yloxy]ethyl moiety fits well into the primary hydrophobic region of the Glennon model, tolerating sterically demanding residues. However, the morpholine ring does not fulfill the requirements to address the second hydrophobic region.

Ligands **8** with excellent $\sigma_1$ receptor binding affinity and selectivity were further evaluated for their activity at the hERG channel and for efficacy in mouse models of neuropathic pain. Naphthylpyrazole **8c** proved to be the most promising candidate with regard to metabolic stability, interaction with the hERG channel ($IC_{50} > 10$ μM), and analgesic activity in different pain models (Diaz et al. 2012). It was found that **8c** shows dose-dependent analgesic effects in both the capsaicin-induced hypersensitivity and the formalin-induced pain model. In the partial sciatic nerve ligation mouse model, **8c** shows dose-dependent inhibition of

thermal hypersensitivity and mechanical allodynia, comparable to the effects of pregabalin, the gold-standard for the treatment of neuropathic pain.

The selectivity of **8c** towards 170 other targets including various receptors and ion channels was shown. With the exception of moderate affinity for the human serotonin 5-$HT_{2B}$ receptor ($K_i$(5-$HT_{2B}$) = 328 nM) other targets were not engaged by **8c**. The antagonist profile of **8c** was verified using phenytoin as an allosteric modulator of $\sigma_1$.

The chemical properties of **8c** meet Lipinski's "rule of five." The pharmacokinetic properties were evaluated in mice. Due to the acceptable solubility and high metabolic stability, a good oral bioavailability can be assumed.

In light of all of the aforementioned properties, **8c** entered clinical trials. Passing the single and multiple dose phase I clinical study provided proof-of-concept that **8c** is safe and well tolerated by healthy humans. Thus, the development of **8c** will be continued into phase II clinical trials (Abadias et al. 2013).

## 10 3,4-Dihydro-2(1*H*)-quinolones

3,4-Dihydro-2(1*H*)-quinolones **9** were developed following the idea of combining a piperidine or morpholine basic element (as realized in the $\sigma_1$ receptor antagonist **8c**) with the quinolone scaffold, which was identified as the interacting element at the $\sigma_1$ receptor (Oshiro et al. 2000). The aim was to obtain compounds with high affinity for the $\sigma_1$ receptor and potent anti-nociceptive properties as shown for S1RA.

For the synthesis of quinolones **9**, 7-hydroxyquinolone **29** was alkylated with dibromoalkans with various length of the alkyl group (Scheme 8). Subsequent reaction with morpholine or piperidine led to the amines **30**, which were converted into 1-alkylated quinolones **9** by reaction with benzyl bromides or iodomethane in presence of NaH (Lan et al. 2014).

The $\sigma_1$ and $\sigma_2$ affinity of quinolones **9** was determined in competition experiments using guinea pig brain membrane preparations (Table 8).

The distance between the quinolone scaffold and the morpholine ring has a strong impact on $\sigma_1$ binding affinity. Whereas **9a** with an ethylene spacer has negligible affinity for $\sigma_1$ ($K_i(\sigma_1) > 2{,}000$ nM), the corresponding homolog **9b** bearing three $CH_2$ moieties in the side chain binds $\sigma_1$ with high affinity ($K_i(\sigma_1) = 14.8$ nM). Elongation by introduction of additional methylene moieties

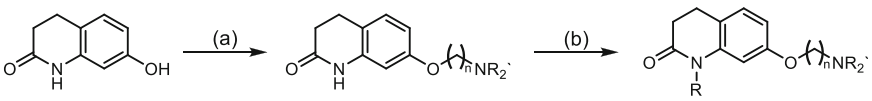


**Scheme 8** Synthesis of quinolones **9**. Reagents and reaction conditions (**a**) (1) $Br(CH_2)_nBr$, $K_2CO_3$, acetone, reflux; (2) $HNR_2$, $K_2CO_3$, KI, $CH_3CN$, reflux; (**b**) NaH, DMF or THF, 0–50 °C (Lan et al. 2014)

**Table 8** $\sigma_1$ and $\sigma_2$ binding affinity of 3,4-dihydro-2(1*H*)-quinolinones **9**

| | $R^1$ | *n* | $NR_2'$ | $\sigma_1$ (gp)[a] $K_i$ [nM] ± SEM | $\sigma_2$ (gp)[a] $K_i$ [nM] ± SEM | $\sigma_1$/ $\sigma_2$ selectivity |
|---|---|---|---|---|---|---|
| 9a | $PhCH_2$ | 2 | Morpholine | >2,000 | >2,000 | – |
| 9b | $PhCH_2$ | 3 | Morpholine | 14.8 ± 0.8 | 471 ± 38 | 32 |
| 9c | H | 3 | Piperidine | 89 ± 14 | 288 ± 52 | 3 |
| 9d | $CH_3$ | 3 | Piperidine | 34 ± 3 | 357 ± 131 | 10 |
| 9e | $PhCH_2$ | 3 | Piperidine | 1.84 ± 0.33 | 662 ± 42 | 360 |
| 9f | 4-F-Ph-$CH_2$ | 3 | Piperidine | 1.22 ± 0.45 | 1,301 ± 204 | 1,066 |
| 9 g | $PhCH_2$ | 4 | Morpholine | 60 ± 4.4 | 530 ± 46 | 9 |
| 9 h | $PhCH_2$ | 5 | Morpholine | 88 ± 5.1 | 1,811 ± 37 | 20 |
| 9i | $PhCH_2$ | 6 | Morpholine | 682 ± 31 | 2,000 | – |

[a]Guinea pig brain (gp)

decreased $\sigma_1$ affinity in the order $n = 3 > n = 4 > n = 5 > n = 6$. Compound **9i**, with a hexamethylene linker, had the lowest $\sigma_1$ binding affinity of this set of compounds with a $K_i$ value of 682 nM. Replacement of the morpholine ring of the most potent ligand **9b** of this series by a piperidine ring led to an almost tenfold increase in $\sigma_1$ binding affinity ($K_i(\sigma_1) = 1.84$ nM). For the promising piperidine derivatives, the effect of the quinolinone *N*-substituent on $\sigma_1$ receptor binding was evaluated by synthesizing different substituted analogs **9c**, **9d,** and **9f**. It has been found that small residues led to decreased $\sigma_1$ affinity compared with the *N*-benzyl substituted derivative **9e** ($K_i(\sigma_1) = 1.84$ nM). In the case of substitution with a proton or a methyl group, the $K_i$ values were only 89 nM (**9c**) or 34 nM (**9d**). The substitution of the phenyl ring with an electron-withdrawing fluorine atom led to a slight increase in $\sigma_1$ binding affinity (**9f**, $K_i(\sigma_1) = 1.22$ nM).

Regarding $\sigma_1/\sigma_2$ selectivity, it was found that the most potent $\sigma_1$ ligand **9f** has also the highest selectivity with a $\sigma_2$ $K_i > 1{,}000$ nM. For the piperidine derivatives **9c-f**, the $\sigma_2$ affinity increased with decreased size of substituents. The secondary lactam **9c** shows the highest $\sigma_2$ affinity and the lowest $\sigma_1/\sigma_2$ selectivity of this set of compounds ($K_i(\sigma_2 = 288$ nM, $\sigma_1/\sigma_2 = 3$). The chain length between the quinolone scaffold and the morpholine residue also influences affinity for the $\sigma_2$ receptor. Compounds **9a** ($n = 2$), **9h** ($n = 5$), and **9i** ($n = 6$) do not show $\sigma_2$ affinity. However, compounds **9b** and **9g** with a trimethylene or tetramethylene linker displayed moderate $\sigma_2$ affinity, with a $K_i$ of approximately 500 nM.

The most potent ligand **9f** was further evaluated for its anti-nociceptive activity in the formalin-induced pain assay. It was found that **9f** dose-dependently reduced both phases of the pain response with $ED_{50}$ values of 49.4 ± 4.1 and 50.5 ± 2.5 mg/kg for the acute phase I and the longer-lasting tonic phase II, respectively. The $\sigma_1$ antagonist activity of **9e** was shown using phenytoin as an allosteric modulator of $\sigma_1$.

## 11 Conclusion

During the past several years, the fields of $\sigma_1$ receptor chemistry and pharmacology have made remarkable progress. Various pharmacophore models of $\sigma_1$ ligands, a 3D homology model of the $\sigma_1$ receptor, its structure in solution (NMR), and its structure in the solid state (X-ray crystallography) have been reported, allowing a closer look at the binding properties of $\sigma_1$ receptors to their ligands. Evidence of $\sigma_1$ as a promising target for the development of new therapeutic approaches has been demonstrated. The $\sigma_1$ antagonist S1RA (**8c**) is currently in clinical trials for the treatment of neuropathic pain. Bicyclic piperazines **2** and **3** inhibit the growth of small cell lung cancer cells (A-427 cells) in a dose-dependent manner, demonstrating their potential as new tumor therapeutics. The (*S*)-configured spirocyclic $\sigma_1$ antagonist **4b** (fluspidine) with a fluoroethyl side chain has been developed as tracer for positron emission tomography (PET) and is currently in clinical trials for imaging and analysis of the brain of patients suffering from major depression.

**Acknowledgement** This work was supported by the *Deutsche Forschungsgemeinschaft*, which is gratefully acknowledged. The authors would like to thank Susann Rath and Melanie Bergkemper for their proofreading and especially Dirk Schepmann for his helpful input in developing this review.

## References

Abadias M, Escriche M, Vaque A, Sust M, Encina G (2013) Safety, tolerability and pharmacokinetics of single and multiple doses of a novel sigma-1 receptor antagonist in three randomized phase I studies. Br J Clin Pharmacol 75:103–117

Bedurftig S, Wunsch B (2004) Chiral, nonracemic (piperazin-2-yl)methanol derivatives with sigma-receptor affinity. Bioorg Med Chem 12:3299–3311

Bermack JE, Debonnel G (2001) Modulation of serotonergic neurotransmission by short- and long-term treatments with sigma ligands. Brit J Pharmacol 134:691–699

Chien CC, Pasternak GW (1993) Functional antagonism of morphine analgesia by (+)-pentazocine-evidence for an anti-opioid sigma(1) system. Eur J Pharmacol 250:R7–R8

Chien CC, Pasternak GW (1994) Selective antagonism of opioid analgesia by a sigma-system. J Pharmacol Exp Ther 271:1583–1590

Chien CC, Pasternak GW (1995) Sigma-antagonists potentiate opioid analgesia in rats. Neurosci Lett 190:137–139

Chu UB, Ruoho AE (2016) Biochemical pharmacology of the sigma-1 receptor. Mol Pharmacol 89:142–153

Diaz JL, Cuberes R, Berrocal J, Contijoch M, Christmann U, Fernandez A et al (2012) Synthesis and biological evaluation of the 1-Arylpyrazole class of sigma(1) receptor antagonists: identification of 4-{2-[5-methyl-1-(naphthalen-2-yl)-1H-pyrazol-3-yloxy]ethyl}morpholine (S1RA, E-52862). J Med Chem 55:8211–8224

Ela C, Barg J, Vogel Z, Hasin Y, Eilam Y (1994) Sigma-receptor ligands modulate contractility, Ca++ influx and beating rate in cultured cardiac myocytes. J Pharmacol Exp Ther 269:1300–1309

Entrena JM, Cobos EJ, Nieto FR, Cendan CM, Gris G, Del Pozo E et al (2009) Sigma-1 receptors are essential for capsaicin-induced mechanical hypersensitivity: studies with selective sigma-1 ligands and sigma-1 knockout mice. Pain 143:252–261

Fischer S, Wiese C, Maestrup EG, Hiller A, Deuther-Conrad W, Scheunemann M et al (2011) Molecular imaging of sigma receptors: synthesis and evaluation of the potent sigma(1) selective radioligand [F-18]fluspidine. Eur J Nucl Med Mol Imaging 38:540–551

Fontanilla D, Johannessen M, Hajipour AR, Cozzi NV, Jackson MB, Ruoho AE (2009) The hallucinogen N,N-dimethyltryptamine (DMT) is an endogenous sigma-1 receptor regulator. Science 323:934–937

Geiger C, Zelenka C, Weigl M, Frohlich R, Wibbeling B, Schepmann D et al (2007) Synthesis of bicyclic sigma receptor ligands with cytotoxic activity. J Med Chem 50:6144–6153

Gilligan PJ, Cain GA, Christos TE, Cook L, Drummond S, Johnson AL et al (1992) Novel piperidine sigma receptor ligands as potential antipsychotic-drugs. J Med Chem 35:4344–4361

Glennon RA (2005) Pharmacophore identification for sigma-1 (sigma(1)) receptor binding: application of the "deconstruction reconstruction elaboration" approach. Mini-Rev Med Chem 5:927–940

Glennon RA, Ablordeppey SY, Ismaiel AM, Elashmawy MB, Fischer JB, Howie KB (1994) Structural features important for sigma(1) receptor-binding. J Med Chem 37:1214–1219

Grosse Maestrup E (2010) Synthese, Charakterisierung und Optimierung fluorierter $\sigma_1$ Rezeptor-Liganden zur Entwicklung eines PET-Tracers für die Hirnforschung. Westfälische Wilhelms-Universität Münster

Hascoet M, Bourin M, Payeur R, Lombet A, Peglion JL (1995) Sigma ligand S14905 and locomotor activity in mice. Eur Neuropsychopharmacol 5:481–489

Hashimoto K, Ishiwata K (2006) Sigma receptor ligands: possible application as therapeutic drugs and as radiopharmaceuticals. Curr Pharm Des 12:3857–3876

Hayashi T, Su TP (2007) Sigma-1 receptor chaperones at the ER-mitochondrion interface regulate Ca2+ signaling and cell survival. Cell 131:596–610

Holl R, Dykstra M, Schneiders M, Frohlich R, Kitamura M, Wurthwein EU et al (2008) Synthesis of 2,5-Diazabicyclo[2.2.2]octanes by Dieckmann analogous cyclization. Aust J Chem 61:914–919

Holl R, Schepmann D, Wunsch B (2012) Homologous piperazine-alcanols: chiral pool synthesis and pharmacological evaluation. MedChemComm 3:673–679

Holl K, Falck E, Kohler J, Schepmann D, Humpf HU, Brust P et al (2013) Synthesis, characterization, and metabolism studies of fluspidine enantiomers. ChemMedChem 8:2047–2056

Hong WM, Werling LL (2000) Evidence that the sigma(1) receptor is not directly coupled to G proteins. Eur J Pharmacol 408:117–125

Ishikawa M, Ishiwata K, Ishii K, Kimura Y, Sakata M, Naganawa M et al (2007) High occupancy of sigma-1 receptors in the human brain after single oral administration of fluvoxamine: a positron emission tomography study using [C-11]SA4503. Biol Psychiatry 62:878–883

James ML, Shen B, Zavaleta CL, Nielsen CH, Mesangeau C, Vuppala PK et al (2012) New positron emission tomography (PET) radioligand for imaging sigma-1 receptors in living subjects. J Med Chem 55:8272–8282

Kohler J, Wunsch B (2006) Lipase catalyzed enantioselective desymmetrization of a prochiral pentane-1,3,5-triol derivative. Tetrahedron-Asymmetry 17:3091–3099

Kohler J, Wunsch B (2012) Conversion of a pentane-1,3,5-triol derivative using lipases as chiral catalysts and possible function of the lid for the regulation of substrate selectivity and enantioselectivity. Biocatal Biotransformation 30:217–225

Kohler J, Bergander K, Fabian J, Schepmann D, Wunsch B (2012) Enantiomerically pure 1,3-Dioxanes as highly selective NMDA and sigma(1) receptor ligands. J Med Chem 55:8953–8957

Laggner C, Schieferer C, Fiechtner B, Poles G, Hoffmann MD, Glossmann H et al (2005) Discovery of high-affinity ligands of sigma(1) receptor, ERG2, and emopamil binding protein by pharmacophore modeling and virtual screening. J Med Chem 48:4754–4764

Lan Y, Chen Y, Xu XQ, Qiu YL, Liu SC, Liu X et al (2014) Synthesis and biological evaluation of a novel sigma-1 receptor antagonist based on 3,4-dihydro-2(1H)-quinolinone scaffold as a potential analgesic. Eur J Med Chem 79:216–230

Laurini E, Dal Col V, Mamolo MG, Zampieri D, Posocco P, Fermeglia M et al (2011) Homology model and docking-based virtual screening for ligands of the sigma(1) receptor. ACS Med Chem Lett 2:834–839

Laurini E, Marson D, Dal Col V, Fermeglia M, Mamolo MG, Zampieri D et al (2012) Another brick in the wall. Validation of the sigma(1) receptor 3D model by computer-assisted design, synthesis, and activity of new sigma(1) ligands. Mol Pharm 9:3107–3126

Lupardus PJ, Wilke RA, Aydar E, Palmer CP, Chen YM, Ruoho AE et al (2000) Membrane-delimited coupling between sigma receptors and K+ channels in rat neurohypophysial terminals requires neither G-protein nor ATP. J Physiol-London 526:527–539

Maestrup EG, Fischer S, Wiese C, Schepmann D, Hiller A, Deuther-Conrad W et al (2009) Evaluation of spirocyclic 3-(3-fluoropropyl)-2-benzofurans as sigma(1) receptor ligands for neuroimaging with positron emission tomography. J Med Chem 52:6062–6072

Maestrup EG, Wiese C, Schepmann D, Brust P, Wunsch B (2011) Synthesis, pharmacological activity and structure affinity relationships of spirocyclic sigma(1) receptor ligands with a (2-fluoroethyl) residue in 3-position. Bioorg Med Chem 19:393–405

Maier CA, Wunsch B (2002a) Novel spiropiperidines as highly potent and subtype selective sigma-receptor ligands. Part 1. J Med Chem 45:438–448

Maier CA,Wunsch B (2002b) Novel sigma receptor ligands. Part 2. SAR of spiro[[2]benzopyran-1,4′-piperidines] and spiro[[2]benzofuran-1,4′-piperidines] with carbon substituents in position 3. J Med Chem 45:4923–4930

Maisonial A, Maestrup EG, Fischer S, Hiller A, Scheunemann M, Wiese C et al (2011) A F-18-labeled fluorobutyl-substituted spirocyclic piperidine derivative as a selective radioligand for PET imaging of sigma(1) receptors. ChemMedChem 6:1401–1410

Maisonial A, Maestrup EG, Wiese C, Hiller A, Schepmann D, Fischer S et al (2012) Synthesis, radiofluorination and pharmacological evaluation of a fluoromethyl spirocyclic PET tracer for central sigma(1) receptors and comparison with fluoroalkyl homologs. Bioorg Med Chem 20:257–269

Mash DC, Zabetian CP (1992) Sigma receptors are associated with cortical limbic areas in the primate brain. Synapse 12:195–205

Matsumoto RR, McCracken KA, Pouw B, Miller J, Bowen WD, Williams W et al (2001) N-alkyl substituted analogs of the sigma receptor ligand BD1008 and traditional sigma receptor ligands affect cocaine-induced convulsions and lethality in mice. Eur J Pharmacol 411:261–273

Ortega-Roldan JL, Ossa F, Amin NT, Schnell JR (2015) Solution NMR studies reveal the location of the second transmembrane domain of the human sigma-1 receptor. FEBS Lett 589:659–665

Oshiro Y, Sakurai Y, Sato S, Kurahashi N, Tanaka T, Kikuchi T et al (2000) 3,4-Dihydro-2(1H)-quinolinone as a novel antidepressant drug: synthesis and pharmacology of 1-[3-[4-(3-chlorophenyl)-1-piperazinyl]propyl]-3,4-dihydro-5-methoxy-2(1H)-quinolinone and its derivatives. J Med Chem 43:177–189

Rack E, Frohlich R, Schepmann D, Wunsch B (2011) Design, synthesis and pharmacological evaluation of spirocyclic sigma(1) receptor ligands with exocyclic amino moiety (increased distance 1). Bioorg Med Chem 19:3141–3151

Rossi D, Pedrali A, Urbano M, Gaggeri R, Serra M, Fernandez L et al (2011) Identification of a potent and selective sigma(1) receptor agonist potentiating NGF-induced neurite outgrowth in PC12 cells. Bioorg Med Chem 19:6210–6224

Ruoho AE, Chu UB, Ramachandran S, Fontanilla D, Mavlyutov T, Hajipour AR (2012) The ligand binding region of the sigma-1 receptor: studies utilizing photoaffinity probes, sphingosine and N-alkylamines. Curr Pharm Des 18:920–929

Samovilova NN, Nagornaya LV, Vinogradov VA (1988) (+)-[H-3]Skf 10,047 binding-sites in rat-liver. Eur J Pharmacol 147:259–264

Schmidt HR, Zheng SD, Gurpinar E, Koehl A, Manglik A, Kruse AC (2016) Crystal structure of the human sigma 1 receptor. Nature 532:527–530

Schwarz S, Pohl P, Zhou GZ (1989) Steroid binding at sigma-opioid receptors. Science 246:1635–1637

Sharkey J, Glen KA, Wolfe S, Kuhar MJ (1988) Cocaine binding at sigma-receptors. Eur J Pharmacol 149:171–174

Skuza G, Rogoz Z (2006) Effect of BD 1047, a sigma(1) receptor antagonist, in the animal models predictive of antipsychotic activity. Pharmacol Rep 58:626–635

Su TP, London ED, Jaffe JH (1988) Steroid binding at sigma-receptors suggests a link between endocrine, nervous, and immune-systems. Science 240:219–221

Sunnam SK (2010) Synthesis of 7,9-diazabicyclo(4.2.2)decanes as conformationally restricted sigma1 ligands and kappa agonists. Westfälische Wilhelms-Universität Münster

Utech T, Kohler J, Buschmann H, Holenz J, Vela JM, Wunsch B (2011) Synthesis and pharmacological evaluation of a potent and selective sigma(1) receptor antagonist with high Antiallodynic activity. Arch Pharm 344:415–421

Wang X, Li Y, Deuther-Conrad W, Xie F, Chen X, Cui MC et al (2013) Synthesis and biological evaluation of F-18 labeled fluoro-oligo-ethoxylated 4-benzylpiperazine derivatives for sigma-1 receptor imaging. Bioorg Med Chem 21:215–222

Weber F (2012) Synthese und Beziehungen zwischen Struktur, σ-Rezeptoraffinität und cytotoxischer Aktivität von überbrückten Piperazin-Derivaten und deren flexibler Analoga. Westfälische Wilhelms-Universität Münster

Weber F, Brune S, Korpis K, Bednarski PJ, Laurini E, Dal Col V et al (2014) Synthesis, pharmacological evaluation, and sigma(1) receptor interaction analysis of hydroxyethyl substituted Piperazines. J Med Chem 57:2884–2894

Weber F, Brune S, Borgel F, Lange C, Korpis K, Bednarski PJ et al (2016) Rigidity versus flexibility: is this an issue in sigma(1) receptor ligand affinity and activity? J Med Chem 59:5505–5519

Weissman AD, Su TP, Hedreen JC, London ED (1988) Sigma-receptors in post-mortem human brains. J Pharmacol Exp Ther 247:29–33

Zampieri D, Mamolo MG, Laurini E, Florio C, Zanette C, Fermeglia M et al (2009) Synthesis, biological evaluation, and three-dimensional in silico pharmacophore model for sigma (1) receptor ligands based on a series of substituted benzo[d]oxazol-2(3H)-one derivatives. J Med Chem 52:5380–5393